

See discussions, stats, and author profiles for this publication at: <https://www.researchgate.net/publication/262021023>

Experimental and kinetic modeling study of 2,5-dimethylfuran pyrolysis at various pressures

ARTICLE in COMBUSTION AND FLAME · OCTOBER 2014

Impact Factor: 3.08 · DOI: 10.1016/j.combustflame.2014.03.022

CITATIONS

7

READS

27

7 AUTHORS, INCLUDING:



Feng Zhang

University of Science and Technology of Ch...

36 PUBLICATIONS 289 CITATIONS

SEE PROFILE



Experimental and kinetic modeling study of 2,5-dimethylfuran pyrolysis at various pressures



Zhanjun Cheng^a, Lili Xing^a, Meirong Zeng^a, Weile Dong^a, Feng Zhang^a, Fei Qi^{a,b}, Yuyang Li^{b,*}

^aNational Synchrotron Radiation Laboratory, University of Science and Technology of China, Hefei, Anhui 230029, PR China

^bState Key Laboratory of Fire Science, University of Science and Technology of China, Hefei, Anhui 230026, PR China

ARTICLE INFO

Article history:

Received 18 October 2013

Received in revised form 30 January 2014

Accepted 31 March 2014

Available online 3 May 2014

Keywords:

2,5-Dimethylfuran

Flow reactor pyrolysis

SVUV-PIMS

Kinetic model

Aromatics formation

ABSTRACT

The pyrolysis of 2,5-dimethylfuran (DMF) in a flow reactor was investigated at various pressures (30, 150 and 760 Torr) by synchrotron vacuum ultraviolet photoionization mass spectrometry (SVUV-PIMS). Dozens of pyrolysis products, especially a series of radicals and aromatics, were identified from the measurement of photoionization efficiency spectra; and their mole fraction profiles were measured at 780–1470 K. Phenol, 1,3-cyclopentadiene, 2-methylfuran, vinylacetylene and 1,3-butadiene were observed with high concentrations in the decomposition of DMF. The pressure-dependent rate constants of the major unimolecular decomposition reactions of DMF were theoretically calculated, and was adopted in the pyrolysis model of DMF with 285 species and 1173 reactions developed in the present work. The model was validated against the species profiles measured in both the present work and the previous pyrolysis studies of DMF. Based on the rate of production and sensitivity analyses, main pathways in the decomposition of DMF and the growth of aromatics were determined. The unimolecular decomposition to produce CH_3CHCCH and acetyl radicals, H-atom abstraction to produce 5-methyl-2-furanylmethyl radical, ipso substitution by H-atom to produce 2-methylfuran and H-atom attack to produce 1,3-butadiene and acetyl radical were concluded to dominate the primary decomposition of DMF. Further decomposition of 5-methyl-2-furanylmethyl radical leads to great production of phenol and 1,3-cyclopentadiene which can be readily converted to precursors of large aromatics such as cyclopentadienyl radical, phenyl radical and benzene. As a result, the formation of aromatics in the pyrolysis of DMF is promoted compared with the pyrolysis of cyclohexane and methylcyclohexane under very close conditions. This observation implies the potentially high sooty tendency of DMF, and emphasizes the necessity to investigate the soot behavior and soot formation mechanism in DMF combustion for the potential application of DMF as an alternative engine fuel.

© 2014 The Combustion Institute. Published by Elsevier Inc. All rights reserved.

1. Introduction

As second-generation biofuels, furan family, including furan, 2-methylfuran (MF) and 2,5-dimethylfuran (DMF), have received more and more attentions because of the rapid consumption of fossil fuels and the potential for large scale industrial synthesis from carbohydrate feedstocks such as fructose, glucose and cellulose [1–3]. Among furan family, DMF is of special interest due to the following reasons. First, DMF is a very promising additive of gasoline due to its similar physical and chemical properties to gasoline [4]. Compared to the first generation biofuel like ethanol, DMF has 40% greater energy density, 15 K higher boiling point, almost null water solubility, and 30% faster laminar flame speeds

[5–7]. Secondly, recent research progresses [1,2] have provided novel production methods of DMF with high efficiency which consume much lower energy than the production of ethanol by fermentation. However, the resonantly stabilized heterocyclic structure of DMF [8] leads to extraordinarily complicated reaction processes in its combustion compared with the combustion of bio-alcohol fuels. Its complex molecular structure is also responsible for the characteristics of DMF in the decomposition, oxidation and pollutant formation processes which are tightly related to the practical application of DMF as a transportation fuel or fuel additive. Recognizing the complexity of DMF chemistry, investigations on the pyrolysis of DMF are desired for both understanding the thermal decomposition mechanism of DMF and developing the kinetic model of DMF combustion. Therefore the aim of the present work is to investigate the pyrolysis chemistry of DMF.

* Corresponding author.

E-mail address: yuygli@ustc.edu.cn (Y. Li).

There are many experimental [5,6,9–21] and theoretical [8,17,22–26] investigations on the pyrolysis and oxidation chemistry of DMF, especially in recent three years. As summarized in Table 1, the experimental studies include the speciation in pyrolysis [9,10,16,19], oxidation [19] and flames [11,20] and the measurements of global combustion parameters such as ignition delay times [18,19], laminar burning velocities [5,6] and engine emissions [12,15,21]. Due to the specific aim of the present work, only previous pyrolysis studies of DMF will be reviewed here. Flow reactor and shock tube are the most frequently used equipments in the pyrolysis experiments of DMF. The earliest experimental investigation on DMF pyrolysis was performed in an electrically heated flow reactor at very low pressure (1 mTorr) by Grela et al. [9] in 1985 using an on-line electron-impact ionization mass spectrometry. They proposed that DMF decomposes via two pathways to produce $C_6H_6 + H_2O$ and $C_5H_8 + CO$. Recently, Djokic et al. [16] used an electrically heated flow reactor with 1.475 m length to study the pyrolysis of DMF from 873 to 1098 K at 1.7 bar. Stable products were identified by an on-line two-dimensional gas chromatograph (GC) combined with a time-of-flight mass spectrometer (TOF-MS). They concluded that the high tendency to form monocyclic aromatic hydrocarbons (MAHs) and polycyclic aromatic hydrocarbons (PAHs) in DMF pyrolysis is due to the large yields of 1,3-cyclopentadiene. Among the shock tube studies, Lifshitz et al. [10] studied the pyrolysis of DMF behind reflected shock waves at temperatures from 1070 to 1370 K and pressures from 2 to 3 atm using GC in 1998. They evaluated the global decomposition rate constants of DMF based on the experimental results. Friese et al. [14] studied the pyrolysis of DMF behind reflected shock waves from 1280 to 1520 K using the atom resonance absorption spectrometry (ARAS) to detect H-atom. They also used ARAS to investigate the $DMF + H$ reactions at temperatures from 970 to 1240 K and pressures of 1.6 and 4.8 bar [14,17]. Overall rate constants of $DMF \rightarrow H +$ products and $DMF + H \rightarrow$ products were derived from the concentration-time profiles of H-atom. In a very recent work, Somers et al. [19] performed a shock tube pyrolysis experiment under very close conditions to the work of Lifshitz et al. [10].

There are scarcely any theoretical studies for the thermal decomposition of DMF before 2011. From then on, several groups

have performed a series of theoretical investigations on the unimolecular decomposition and radical attack of DMF [17,22,23,25,26], as well as the decomposition of its H-loss product 5-methyl-2-furanylmethyl radical [24]. The calculated results by Sirjean and Fournet [25] reveal that the most important chain initiation reactions in DMF pyrolysis are the carbene rearrangement of DMF via 3,2-H-atom transfer and the initial C–H bond fission in the CH_3 groups.

These studies provide valuable experimental and theoretical results for the development of DMF models. Along with the shock tube pyrolysis investigation, Lifshitz et al. [10] developed a simple pyrolysis model of DMF containing 50 species and 181 reactions, and validated the model against their measured mole fraction profiles of pyrolysis species. Recently, Sirjean et al. [18] developed a DMF model based on their theoretical work on the thermal decomposition of DMF. They used the pyrolysis data from Lifshitz et al. [10] to validate the pyrolysis submechanism, and also measured the ignition delay times of DMF at temperatures from 1300 to 1831 K and pressures of 1 and 4 bar to validate the oxidation submechanism. More recently, Somers et al. [19] developed a detailed DMF model including 545 species and 2768 reactions based on their previous MF model [27] and the DMF model of Sirjean et al. [18]. The pyrolysis data from their own work, Lifshitz et al. [10] and Djokic et al. [16] were used to validate the pyrolysis submechanism. They also measured the species profiles in jet stirred reactor oxidation, ignition delay times and laminar burning velocities to validate the oxidation submechanism, along with oxidation data of DMF in literature. Besides, Togbe et al. [20] developed a DMF model based on the model of Sirjean et al. [18] and validated it against their premixed flame data at low pressure.

It is recognized that most of previous experimental investigations on the pyrolysis of DMF used GC techniques to detect pyrolysis species and measure their concentration profiles. However GC techniques can hardly provide information on free radicals which play significant roles in the thermal decomposition processes. On the other hand, only Djokic et al. [16] reported measurements of aromatic hydrocarbons beside benzene in previous pyrolysis and combustion studies of DMF, while attentions on modeling the formation of aromatics in DMF combustion are still lacking.

Table 1
A list of experimental investigations on DMF combustion in literature.

Year	Temperature (K)	Pressure	Reactor	References
<i>Pyrolysis</i>				
1985	1050–1270	1 mTorr	Flow reactor	Grela et al. [9]
1998	1070–1370	2–3 atm	Shock tube	Lifshitz et al. [10]
2011	1280–1520	1.6, 4.7 bar	Shock tube	Friese et al. [14]
2013	873–1098	1.7 bar	Flow reactor	Djokic et al. [16]
2013	1200–1350	2–2.5 atm	Shock tube	Somers et al. [19]
Year	Temperature (K)	Pressure	Equivalence ratio	References
<i>Oxidation</i>				
2013	770–1220	10 atm	0.5, 1.0, 2.0	Somers et al. [19]
Year	Equivalence ratio	Pressure	References	
<i>Premixed laminar flame</i>				
2009	2.0	30 Torr	Wu et al. [11]	
2013	1.0, 1.7	20, 40 mbar	Togb�� et al. [20]	
Year	Temperature (K)	Pressure	Equivalence ratio	References
<i>Ignition delay times</i>				
2013	1300–1831	1, 4 bar	0.5, 1.0, 1.5	Sirjean et al. [18]
2013	1350–1800	1 atm	0.5, 1.0, 2.0	Somers et al. [19]
Year	Equivalence ratio	Pressure	References	
<i>Laminar burning velocity</i>				
2010	0.6–2.0	0.1 MPa	Tian et al. [5]	
2011	0.8–1.5	0.1, 0.25, 0.5, 0.75 MPa	Wu et al. [6]	
2013	0.6–1.6	1 atm	Somers et al. [19]	

Furthermore, most of previous experimental investigations were carried out at single pressure conditions or narrow pressure ranges, which limits the validation on the rate constants of the pressure-dependent reactions. In the present work, synchrotron vacuum ultraviolet photoionization mass spectrometry (SVUV-PIMS) was used to detect different types of products in the flow reactor pyrolysis of DMF. Three pressures (30, 150 and 760 Torr) were selected to investigate the pressure effects in the pyrolysis of DMF. Furthermore, a detailed pyrolysis model of DMF focused on both the decomposition of DMF and formation of aromatics was developed based on recent theoretical and modeling progresses, especially the calculated rate constants of primary decomposition reactions of DMF in the present work. The model was validated against the pyrolysis data of DMF both in the present work and in literature.

2. Experimental method

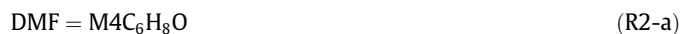
The experiments were conducted at National Synchrotron Radiation Laboratory, Hefei, China. Detailed descriptions of the beamlines and pyrolysis apparatus were reported in our previous work [28–31]. Figure 1 shows the schematic diagram of the pyrolysis apparatus. A flow tube with 150 mm length heated was mounted inside a high temperature furnace in the pyrolysis chamber. The flow tube was made of α -alumina to reduce surface catalytic effects [32], and relevant discussion can be found in Supplementary Materials. A small inner diameter (7.0 mm) was used to strengthen the radial diffusion effects, decrease the radial concentration gradients and reach adequately homogenous reaction circumstances for modeling purpose according to the

experiences in previous laminar flow reactor experiments [33–35]. The inlet flow rate of 2% DMF in Ar was 1000 standard cubic centimeters per minute (SCCM) at all pressures. DMF with a purity of ~99% was synthesized by Beijing LYS Chemicals CO., Ltd., China, and Ar with a purity of 99.99% was purchased from Nanjing Special Gases Factory Ltd., China.

The pyrolysis species were sampled at 10 mm downstream of the reactor outlet by a quartz nozzle. The formed molecular beam entered the photoionization chamber through a nickel skimmer and was ionized by the synchrotron VUV light in the photoionization region. The ions were detected and analyzed by a home-made reflectron TOF-MS. The centerline temperature distributions along the flow reactor under different heating temperatures were measured by an S-type thermocouple. Every temperature profile is identified by its maximum value (T_{\max}) which has uncertainties within ± 30 K. T_{\max} is also used as the experimental temperature in the following discussion, as shown in Fig. 1. The methods of temperature distribution measurement along the centerline of flow tube and mole fraction evaluation have been introduced in detail in our previous work [30,36–38], and the temperature profiles are presented in Supplementary Materials. The uncertainties of measured mole fractions are generally within $\pm 25\%$ for pyrolysis products with known photoionization cross sections and a factor of 2 for those with estimated photoionization cross sections.

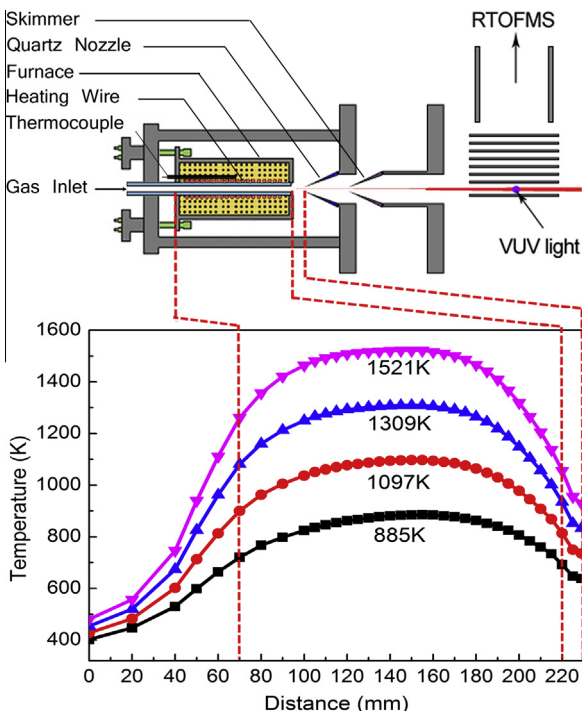
3. Theoretical calculation

Sirjean and Fournet [25] calculated the comprehensive decomposition pathways of DMF by using the CBS-QB3 method. Based on their theoretical calculations, a small reaction mechanism for the thermal decomposition of DMF was built to evaluate the contributions of primary pathways to the DMF decomposition. The results indicated that two pathways dominate the unimolecular decomposition of DMF. One is the initial C–H bond fission in the CH_3 groups leading to the resonantly stabilized 5-methyl-2-furanyl methyl radical ($\text{R1C}_6\text{H}_7\text{O}$) and the H-atom (R1). The other one is the carbene rearrangement of DMF via 3,2-H-atom transfer to produce hexa-3,4-dien-2-one ($\text{M4C}_6\text{H}_8\text{O}$) (R2-a) which ultimately yields CH_3CHCCH ($\text{C}_4\text{H}_5\text{-1s}$) and acetyl (CH_3CO) radicals (R2-b), and can be written as the global form $\text{DMF} = \text{C}_4\text{H}_5\text{-1s} + \text{CH}_3\text{CO}$ (R2). The high pressure limit (HPL) rate constants of the barrierless dissociation reactions R1 and R2-b were estimated from the rate constants of their reverse association reactions which were referred to those of benzyl + H [39] and the average value of $\text{CH}_3\text{CO} + \text{alkyl/alkenyl}$ radicals (CH_3 , C_2H_3 , C_2H_5 , $n\text{-C}_3\text{H}_7$ and $i\text{-C}_4\text{H}_9$) [40–42], respectively. Moreover, the fall-off effects of these pathways were estimated from those of the C–H and C–C bond fission reactions of toluene [43].



In order to investigate the pressure effects of R1 and R2 more rigorously, the Inverse Laplace Trans-form (ILT) method [44,45] in the MESMER code [46] was used in the present work. The potential energy surfaces of the two pathways were repeated by using the CBS-QB3 method. All quantum chemistry calculations were carried out with the Gaussian 09 program [47]. The carbene intermediate was omitted for simplicity of the kinetic study. The micro-canonical rate constants of barrierless dissociation reactions are deduced by inverse Laplace transformation of the HPL rate constant of association reactions. The ILT calculation relies on both

Fig. 1. (a) Schematic diagram of the pyrolysis apparatus with a molecular-beam sampling system and a reflectron TOF-MS [30,37,54]. The red circles inside the furnace denote an electronically heating wire with the length of 150 mm in the present work. A tungsten–rhenium (W–Re) thermocouple is put close to the middle region of the heating wire. (b) Examples of temperature profiles along the centerline of the flow tube measured by moving an S-type thermocouple (not shown in the figure) from the tube inlet to the sampling point of the quartz nozzle. (For interpretation of the references to colour in this figure legend, the reader is referred to the web version of this article.)



the equilibrium constants calculated at the CBS-QB3 level of theory and the HPL rate constants of association reactions. According to the association rate constants of $\text{CH}_3\text{CO} + \text{alkyl/alkenyl radicals}$ to produce ketones [40–42] and the bond dissociation energies (BDEs) of ketones [48], the association rate constants were found to change inversely to the BDEs of ketones. Therefore, the association rate constant of $\text{C}_4\text{H}_5\text{-1s} + \text{CH}_3\text{CO}$ was estimated to $3.0\text{E+13 cm}^3 \text{ mol}^{-1} \text{ s}^{-1}$ which is about 1.3–1.7 times of those of $\text{CH}_3\text{CO} + \text{alkyl/alkenyl radicals}$ [40–42], considering the 7–22 kcal/mol lower BDE of $\text{M4C}_6\text{H}_8\text{O}$ (74.3 kcal/mol [25]) than those of other ketones [48]. Similarly, the HPL rate constants of the association of $\text{H} + \text{R1C}_6\text{H}_8\text{O}$ were estimated to be $9.83\text{E+13 T}^{0.07} \text{ EXP}(51.5/\text{RT}) \text{ cm}^3 \text{ mol}^{-1} \text{ s}^{-1}$ by multiplying that of benzyl + H [39] by a factor of 1.5 due to the weaker C–H bond in the methyl groups of DMF (~ 85 kcal/mol) [8] than that of toluene (~ 92 kcal/mol) [49]. With the ILT computation for the barrierless dissociation reactions and the RRKM calculation for the isomerization reactions between DMF and $\text{M4C}_6\text{H}_8\text{O}$, the pressure effects of R1 and R2 were simulated by the master equation method. Low-frequency vibrational models corresponding to internal rotation were treated as hindered rotors. The hindrance potentials were obtained by relaxed scanning every 10 degrees using the M052X/6-31 + G(d,p) method. The Eckart tunneling corrections were also included. The interaction between the reactants and the bath gas Ar was modeled by the Lennard–Jones (L–J) potentials [50]. The L–J parameters were estimated as $\sigma = 3.465 \text{ \AA}$, $\varepsilon = 113.5 \text{ K}$ for Ar; $\sigma = 5.943 \text{ \AA}$, $\varepsilon = 445.1 \text{ K}$ for DMF; and $\sigma = 6.020 \text{ \AA}$, $\varepsilon = 459.0 \text{ K}$ for $\text{M4C}_6\text{H}_8\text{O}$. The collision energy transfer was treated using a single-parameter exponential down mode: $\langle \Delta E_{\text{down}} \rangle = 300 (T/300)^{0.85}$. The calculated pressure-dependent (30, 150, 760, 7600 and 76000 Torr) and temperature-dependent (800–2000 K) rate constants of R1 and R2 are listed in Table 2.

4. Kinetic modeling

In the present work, a detailed pyrolysis model of DMF including 285 species and 1173 reactions was developed. The present model mainly consists of three submechanisms, i.e. the C0–C4 submechanism, the aromatics submechanism and the DMF submechanism. The C0–C4 submechanism was taken from our previous butene model [36] and butanol models [37,51] which were validated against our recent pyrolysis data of butene and butanol isomers. The aromatics submechanism was mainly taken from our recently reported aromatics model which was validated against our recent experimental results of the toluene [52] and ethylbenzene [53] flames and tetralin pyrolysis [54]. The rate constants of reactions in the DMF submechanism were mainly taken from the calculated results of R1 and R2 in the present work, the DMF model from Sirjean et al. [18], the MF model from Somers et al. [27] and furan model from Tian et al. [55]. Table 2 lists the rate coefficients of key reactions in the DMF submechanism and the aromatics submechanism. The chemical structures of important species involved in the DMF submechanism are displayed in Table S1 in the Supplementary Materials. Furthermore, most of the thermodynamic data were taken from previous DMF models [18,24–26], MF model [27], furan model [55] and butanol models [37,51]. The reaction mechanism and thermodynamic data are summarized in Supplementary Materials. The simulation of the flow reactor pyrolysis experiments was performed using the Plug Flow code in the Chemkin-PRO software [56]. The measured temperature profiles along the centerline of the flow tube were used as input parameters in the simulation. The simulated mole fractions of DMF, Ar and products at the final positions under different temperatures were plotted as the simulated mole fraction profiles. The shock tube pyrolysis experiments were simulated by the Closed

Homogeneous Batch code in the Chemkin-Pro software [56] under constant volume conditions. Because transport data are not required input parameters in both codes, they are not included in the present model.

5. Results and discussion

5.1. Pyrolysis of DMF at various pressures

About 50 pyrolysis products, such as radicals, isomers and aromatics, were identified in the present work. Particularly, a series of radicals like methyl radical (CH_3), propargyl radical (C_3H_3), allyl radical (aC_3H_5), cyclopentadienyl radical (C_5H_5), benzyl radical ($\text{C}_6\text{H}_5\text{CH}_2$) and indenyl radical (C_9H_7) were observed at 30 Torr. In this section, validation of the present model was performed by reproducing the mole fraction profiles of observed pyrolysis species, and the discussion will be focused on the decomposition of DMF and the formation of aromatics.

5.1.1. Decomposition of DMF

The experimental and simulated mole fraction profiles of DMF, vinylacetylene (C_4H_4), CH_3 , carbon monoxide (CO), methane (CH_4) and hydrogen (H_2) at various pressures are illustrated in Fig. 2. To understand the decomposition processes of DMF at different pressures, rate of production (ROP) analysis and sensitivity analysis were performed at 1389 K, 30 Torr and 1176 K, 760 Torr where around 75% of DMF is consumed and most intermediates have relatively high mole fractions. According to the ROP analysis, the main reaction pathways in the decomposition of DMF at 30 and 760 Torr were found to be very similar. Therefore only the reaction network in the decomposition of DMF at 30 Torr is exhibited in Fig. 3, while that in 760 Torr can be found in Fig. S4 in the Supplementary Materials. For pathways with high reaction fluxes, their percentages in total reaction flux from DMF are labeled. Furthermore, Fig. 4 shows the sensitivity analysis of DMF at 1389 K, 30 Torr and 1176 K, 760 Torr.

The ROP analysis indicates that the consumption of DMF is mainly controlled by the unimolecular decomposition reactions and radical attack reactions. The most important unimolecular decomposition pathway of DMF is R2 which produces $\text{C}_4\text{H}_5\text{-1s}$ and CH_3CO . The contributions of this pathway to the consumption of DMF are 12% and 5% at 30 and 760 Torr, respectively, in contrast to 4% and 1% at 30 and 760 Torr for the initial C–H bond fission in the CH_3 groups (R1). This is consistent with the conclusions of Sirjean et al. [18] and Somers et al. [19] by simulating the shock tube pyrolysis data of DMF from Lifshitz et al. [10]. The $\text{C}_4\text{H}_5\text{-1s}$ radical can quickly convert to C_4H_4 , which contributes over 60% to the production of C_4H_4 at both 30 and 760 Torr. Figure 2b shows the experimental and simulated results of C_4H_4 . By comparing the measured concentrations of C_4H_4 at the same conversion rate of DMF (i.e. 75%) at three pressures, it is observed that the concentration of C_4H_4 decreases dramatically as the pressure increases, corresponding to the decreasing contribution of unimolecular decomposition reactions to the consumption of DMF. The other product from R2, CH_3CO radical, is mainly consumed by a unimolecular decomposition reaction to produce CH_3 and CO, which is also a main formation pathway of CH_3 and CO at both 30 and 760 Torr.

As a result of the unimolecular decomposition of DMF, small radicals like H-atom and CH_3 radical are formed and can attack DMF to accelerate its decomposition (e.g. R3–R6). The ROP analysis shows that the radical attack reactions contribute about 80% to the consumption of DMF at 30 Torr, and their total contribution increases to over 90% at 760 Torr. The H-atom abstraction reactions, especially those by H-atom and CH_3 radical, afford around

Table 2A list of selected reactions from the present model. Units are s⁻¹, cm³ and cal/mol.

Selected reactions		A	n	E	Pressure (Torr)	References
<i>Reactions of DMF</i>						
R1	DMF = R1C ₆ H ₇ O + H	2.00E+90 6.63E+75 2.08E+58 3.25E+38 1.08E+24	-21.98 -17.63 -12.46 -6.61 -2.37	1.25E+05 1.19E+05 1.10E+05 9.94E+04 9.15E+04	30 150 760 7600 76000	Present work Present work Present work Present work Present work
R2	DMF = C ₄ H ₅ -1s + CH ₃ CO	9.67E+119 1.97E+114 5.52E+107 5.11E+97 6.84E+90	-30.16 -28.38 -26.40 -23.41 -21.39	1.47E+05 1.45E+05 1.42E+05 1.37E+05 1.33E+05	30 150 760 7600 76000	Present work Present work Present work Present work Present work
R3	DMF + H = R1C ₆ H ₇ O + H ₂	3.10E+05	2.70	3.43E+03	-	[18]
R4	DMF + CH ₃ = R1C ₆ H ₇ O + CH ₄	6.99E+01	3.37	7.08E+03	-	[18]
R5	DMF + H = MF + CH ₃	3.88E+19 3.06E+22 1.55E+22 3.91E+25	-1.61 -2.39 -2.27 -3.18	9.66E+03 1.24E+04 1.32E+04 1.67E+04	7.6 76 760 7600	[26] ^a
R6	DMF + H = C ₄ H ₆ + CH ₃ CO	1.34E+32 7.21E+41 1.72E+53 2.85E+67	-5.24 -7.93 -11.04 -14.87	1.70E+04 2.48E+04 3.50E+04 4.94E+04	7.6 76 760 7600	[26]
R7	DMF + C ₅ H ₅ = R1C ₆ H ₇ O + C ₅ H ₆	1.37E+00	3.85	1.44E+04	-	[18]
R8	C ₆ H ₅ OH = C ₅ H ₆ + CO	8.62E+15	-0.61	7.41E+04	-	[58]
R9	C ₆ H ₆ + OH = C ₆ H ₅ OH + H	4.99E+08 8.21E+13 6.68E+20	1.31 -0.13 -2.02	6.54E+03 1.07E+04 1.68E+04	760 7600 76000	[66]
R10	C ₆ H ₅ OH + H = C ₆ H ₅ O + H ₂ C ₆ H ₅ OH + CH ₃ = C ₆ H ₅ O + CH ₄	1.15E+14 1.80E+11	0.00 0.00	1.24E+04 7.70E+03	- -	[67] [68]
R11	C ₆ H ₅ O = C ₅ H ₅ + CO	1.17E+81 1.47E+77 2.67E+72 1.93E+29	-19.66 -18.45 -16.95 -4.45	9.27E+04 9.15E+04 9.04E+04 6.44E+04	380 684 1900 76000	[69]
R12	MF + C ₅ H ₅ = furylCH ₂ + C ₅ H ₆	6.86E-01	3.85	1.44E+04	-	[18]
R13	C ₃ H ₃ + C ₃ H ₃ = C ₆ H ₆	1.82E+74 3.16E+55 3.89E+50	-18.14 -12.55 -11.01	3.19E+04 2.23E+04 2.03E+04	30 760 7600	[60]
R14	C ₃ H ₃ + C ₃ H ₃ = C ₆ H ₅ + H Duplicate C ₃ H ₃ + C ₃ H ₃ = C ₆ H ₅ + H Duplicate	1.58E+54 1.38E+34	-11.94 -6.72	2.90E+04 1.38E+04	30 30	[60]
R15	C ₆ H ₅ CH ₃ + OH = C ₆ H ₅ OH + CH ₃	7.83E+02	2.88	3.22E+03	-	[70]
R16	C ₃ H ₃ + C ₄ H ₆ = C ₆ H ₅ CH ₃ + H	6.53E+05	1.28	-4.61E+03	-	[71]
R17	C ₆ H ₅ CH ₃ (+M) = C ₆ H ₅ CH ₂ + H (+M) LOW/ TROE/6.55E-02	2.78E+15 1.00E+98 1.51E+01	0.17 -22.86 1.00E+10	9.12E+04 9.99E+04 7.60E+07/	- - -	[43]
R18	C ₆ H ₅ CH ₃ (+M) = C ₆ H ₅ + CH ₃ (+M) LOW/ TROE/7.05E-01	1.95E+27 1.00E+98 1.00E+10	-3.16 -22.97 4.60E+02	1.07E+05 1.22E+05 8.21E+09/	- - -	[43]
R19	C ₆ H ₅ CH ₃ + H = C ₆ H ₅ CH ₂ + H ₂ C ₆ H ₅ CH ₃ + CH ₃ = C ₆ H ₅ CH ₂ + CH ₄	6.47E+00 2.94E+11	3.98 0.00	3.40E+03 9.25E+03	- -	[72] [73]
R20	C ₆ H ₅ CH ₂ + H = C ₆ H ₅ + CH ₃	5.83E+67	-14.15	6.83E+04	760	[43]
R21	C ₆ H ₅ + C ₂ H ₂ = C ₆ H ₅ C ₂ H + H	3.98E+13	0.00	1.01E+04	-	[74]
R22	C ₆ H ₅ + C ₂ H ₄ = C ₆ H ₅ C ₂ H ₃ + H	2.51E+12	0.00	6.19E+03	-	[74]
R23	C ₅ H ₅ + C ₃ H ₃ = C ₆ H ₅ C ₂ H ₃	3.64E+73 6.32E+54 7.78E+49	-18.14 -12.55 -11.01	3.19E+04 2.23E+04 2.03E+04	30 760 7600	[60] ^b

Note:

^a Divided by a factor of 1.5 based on the validation against the present work and pyrolysis data of DMF in literature.^b Referred to C₃H₃ + C₃H₃ = C₆H₆ [60] and divided by a factor of 5 in the present work.

three fifths in the total reaction fluxes of radical attack reactions at both 30 and 760 Torr. Because of the special chemical structure, only two types of H-atoms exist in DMF, i.e. six H-atoms in the CH₃ groups and two H-atoms on the furan ring. As a result, there

are two kinds of H-atom abstraction reactions for DMF. One is the H-atom abstraction from the CH₃ groups to produce R1C₆H₇O radical, and the other one from the furan ring to produce the vinylic C₆H₇O radical (DMF-3-yl). It is concluded that the H-atom

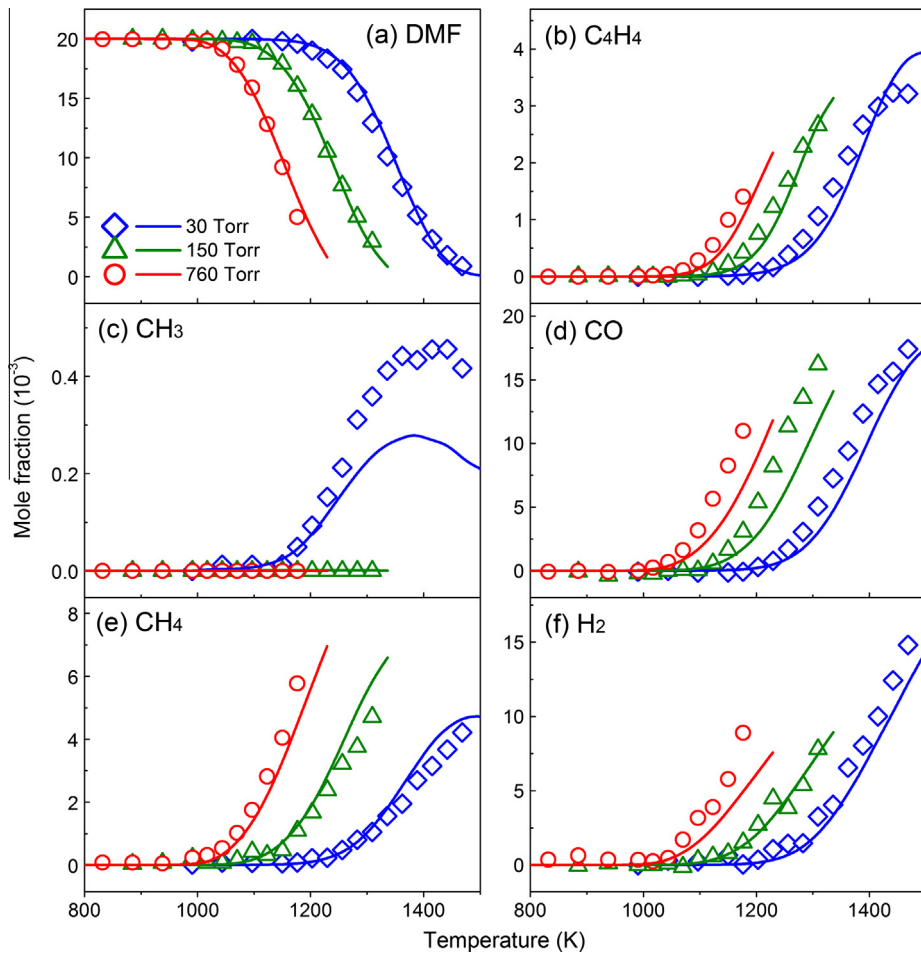


Fig. 2. Experimental (symbols) and simulated (lines) mole fraction profiles of (a) DMF, (b) vinylacetylene (C_4H_4), (c) methyl radical (CH_3), (d) carbon monoxide (CO), (e) methane (CH_4) and (f) hydrogen (H_2) in DMF pyrolysis at various pressures.

abstraction reactions from the CH_3 groups occupy almost all reaction flux among the H-atom abstraction reactions of DMF. This is in accordance with the fact that the C-H bond in the CH_3 groups is the weakest bond in DMF [8]. As a result, about half of DMF (50% at 30 Torr and 57% at 760 Torr) decomposes through the H-atom abstraction reactions by H-atom and CH_3 radical (R3) and (R4), and produces H_2 and CH_4 along with $R1C_6H_7O$. Experimental and simulated mole fraction profiles of H_2 and CH_4 are shown in Fig. 2.



The sensitivity analysis of DMF in Fig. 4 also reveals the importance of the unimolecular decomposition and H-atom abstraction reactions for the decomposition of DMF at both 30 and 760 Torr. In general, the decomposition of DMF is very sensitive to the unimolecular reactions (especially R2) at both pressures, and the total influence of H-atom abstraction reactions on the decomposition of DMF increases as the pressure elevates.

Figure 5 compares the simulated results of DMF and C_4H_4 at 30 and 760 Torr by the present model and recent DMF models of Sirjean et al. [18] (referred as the Sirjean model) and Somers et al. [19] (referred as the Somers model). At 760 Torr, the initial decomposition temperature of DMF can be captured by three models.

However, the simulated decomposition rate of DMF by the Somers model is faster than those by the other models. The ROP and sensitivity analysis indicates that the fast consumption of DMF by the Somers model mainly results from the over-estimated rate constant of H-atom abstraction of DMF by C_5H_5 attack (R7). For example, at 75% conversion of DMF in the 760 Torr pyrolysis, R7 consumes 12% and 0.5% of DMF by the Somers and Sirjean models, respectively. In the Somers model, R7 was referred to the H-atom abstraction of toluene ($C_6H_5CH_3$) by C_5H_5 radical [57], and the rate constant was doubled considering the two methyl groups in DMF. In the Sirjean and present models, the rate constant of R7 was both taken from the calculated result of the H-atom abstraction of MF by aC_3H_5 radical [18] with the A factor doubled. The rate constants of R7 in the Somers and Sirjean models are plotted in Fig. S5 in the Supplementary Materials. It is observed that the rate constant of R7 in the Somers model is at least an order of magnitude faster than that in the Sirjean model at the temperature region of the 760 Torr experiment. It is noticed that a typo was made in the activation energy term of the $C_6H_5CH_3 + C_5H_5$ reaction in the original literature [57], which reduces the activation energy by 4 kcal/mol and explains the extraordinarily fast rate constant of R7 in the Somers model.



At 30 Torr, it is observed from Fig. 5 that the simulated mole fraction profiles of DMF and C_4H_4 by the Sirjean and Somers models both shift toward lower temperatures compared with the experimental results. According to the ROP and sensitivity analysis,

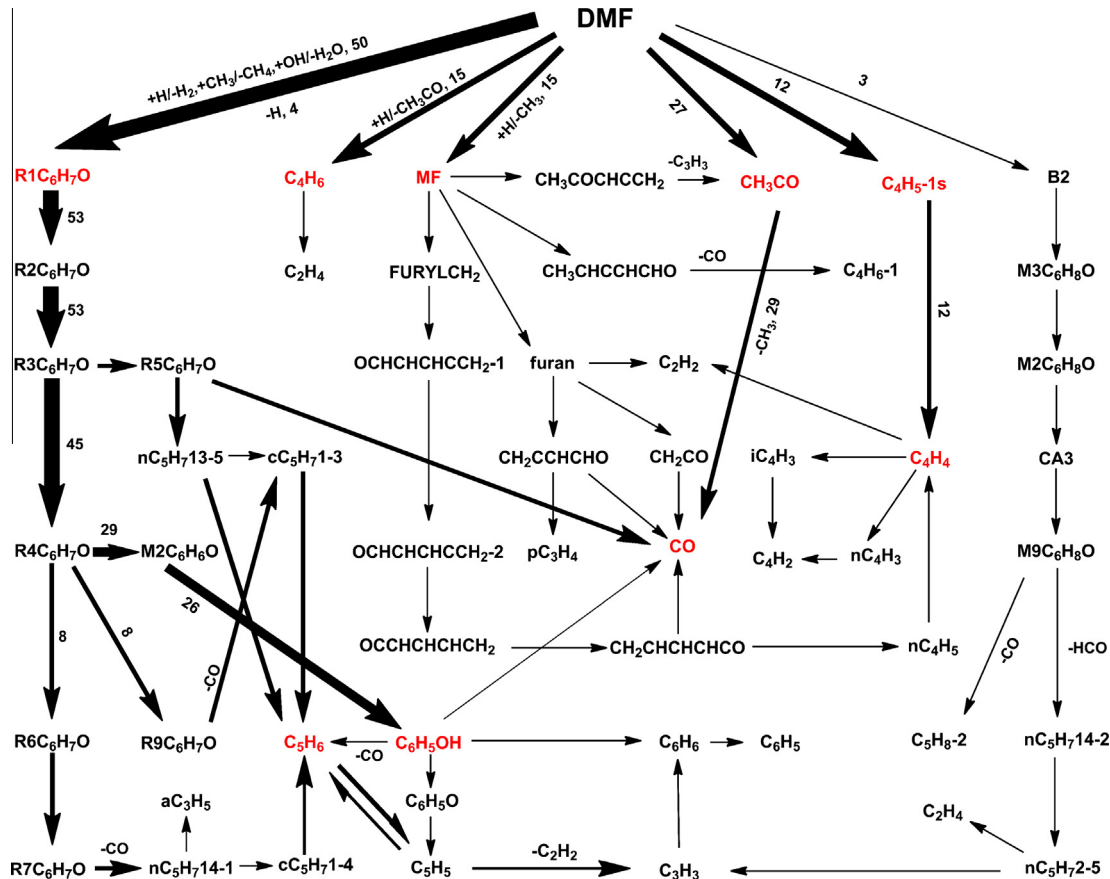


Fig. 3. Reaction network in the decomposition of DMF at 1389 K and 30 Torr. The numbers reflect the percentages of corresponding pathways in total reaction flux.

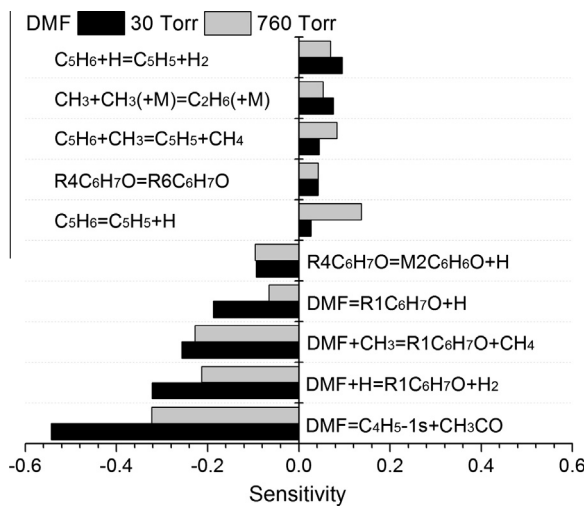


Fig. 4. Sensitivity analysis of DMF at 1389 K, 30 Torr and 1176 K, 760 Torr.

R1 and R2 are very significant for the decomposition of DMF and the formation of major products. In the Sirjean and Somers models, the rate constants of R1 and R2-b were both adopted from the work of Sirjean et al. [18,25]. However, the fall-off effects of these pressure-dependent reactions in their work were estimated from those of C-H and C-C bond fission reactions of toluene [43]. The comparison at 30 Torr in Fig. 5 indicates that this estimation leads to great uncertainties of the pressure effects of these reactions.

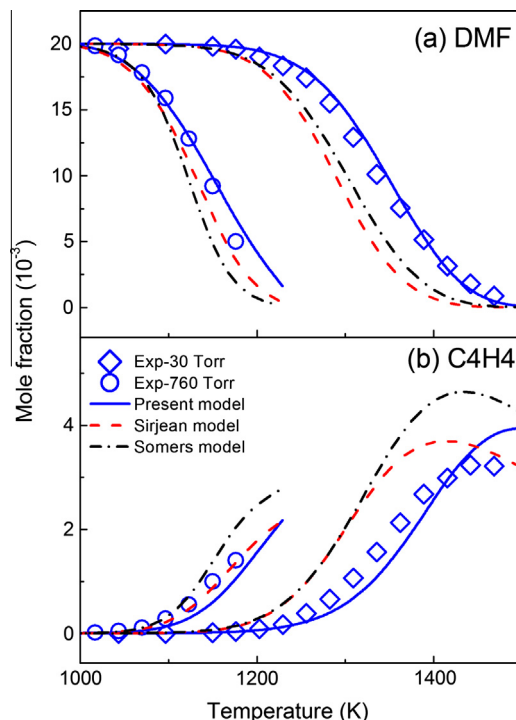


Fig. 5. Comparison of simulated mole fraction profiles of (a) DMF and (b) C_4H_4 by the present model (solid lines), the Sirjean model (dashed lines) and the Somers model (dash dot lines) with experimental results (symbols).

With the calculated pressure-dependent rate constants of R1 and R2 in the present work, the experimental trends of DMF and C₄H₄ at both 30 and 760 Torr can be captured by the present model.

According to the discussion above, R1C₆H₇O radical can be produced from both H-atom abstraction reactions (like R3 and R4) and the initial C–H bond fission in the CH₃ groups (R1), and affords very high reaction flux from DMF, making it the most important primary decomposition product in the combustion of DMF. In the theoretical investigation on the decomposition of R1C₆H₇O radical by Sirjean and Fournet [24], it is concluded that R1C₆H₇O radical mainly suffers a series of unimolecular reactions to produce phenol (C₆H₅OH) and 1,3-cyclopentadiene (C₅H₆). The experimental and simulated mole fraction profiles of C₆H₅OH and C₅H₆ are displayed in Fig. 6a and b, respectively. In the present model, the rate constants of reactions from R1C₆H₇O radical to C₆H₅OH and C₅H₆ were mainly taken from the Sirjean model. Besides, a unimolecular decomposition reaction of C₆H₅OH to produce C₅H₆ and CO calculated by Xu and Lin [58] (R8) was added to the present model.



From Fig. 3, it can be observed that R1C₆H₇O radical is totally consumed by the ring-opening reaction to produce R2C₆H₇O radical. The further internal 1,5-H-transfer reaction of R2C₆H₇O radical produces R3C₆H₇O radical. R3C₆H₇O radical can suffer two branching isomerization reactions to produce R4C₆H₇O and

R5C₆H₇O radicals, and the isomerization to R4C₆H₇O radical has higher contributions at both 30 and 760 Torr. There are three decomposition pathways of R4C₆H₇O radical which finally produce C₆H₅OH and C₅H₆. The reaction sequence R4C₆H₇O → M2C₆H₆–O → C₆H₅OH consumes 64% and 71% of R4C₆H₇O radical at 30 and 760 Torr, respectively, and produces almost all C₆H₅OH at both pressures. C₆H₅OH has three different types of main decomposition pathways, including the unimolecular decomposition (R8), ipso substitution by H-atom to produce benzene (C₆H₆) (R9) and H-atom abstraction reactions by small radicals to produce phenoxyl radical (C₆H₅O) (R10). At 30 Torr, the decomposition of C₆H₅OH is dominated by R8 (61%), while only 18% of C₆H₅OH suffers R10 to produce C₆H₅O radical. At 760 Torr, the dominant decomposition pathway of C₆H₅OH becomes R10 (52%), while R8 consumes only 26% of C₆H₅OH due to the reduced contributions of unimolecular decomposition reactions at elevated pressures. The contributions of R9 to the consumption of C₆H₅OH are similar at 30 Torr (14%) and 760 Torr (18%). The rest two consumption pathways of R4C₆H₇O radical via R6C₆H₇O and R9C₆H₇O radicals, as well as R8 and the main decomposition pathway of R5C₆H₇O radical, control the formation of C₅H₆ at both 30 and 760 Torr. As seen from Fig. 3, the consumption of C₆H₅O radical is almost totally controlled by the CO elimination reaction to generate C₅H₅ radical (R11) which can also be generated from the decomposition of C₅H₆. The decomposition of C₅H₅ radical produces C₃H₃ radical and acetylene (C₂H₂). Furthermore, nC₅H₁₄–1 radical from the

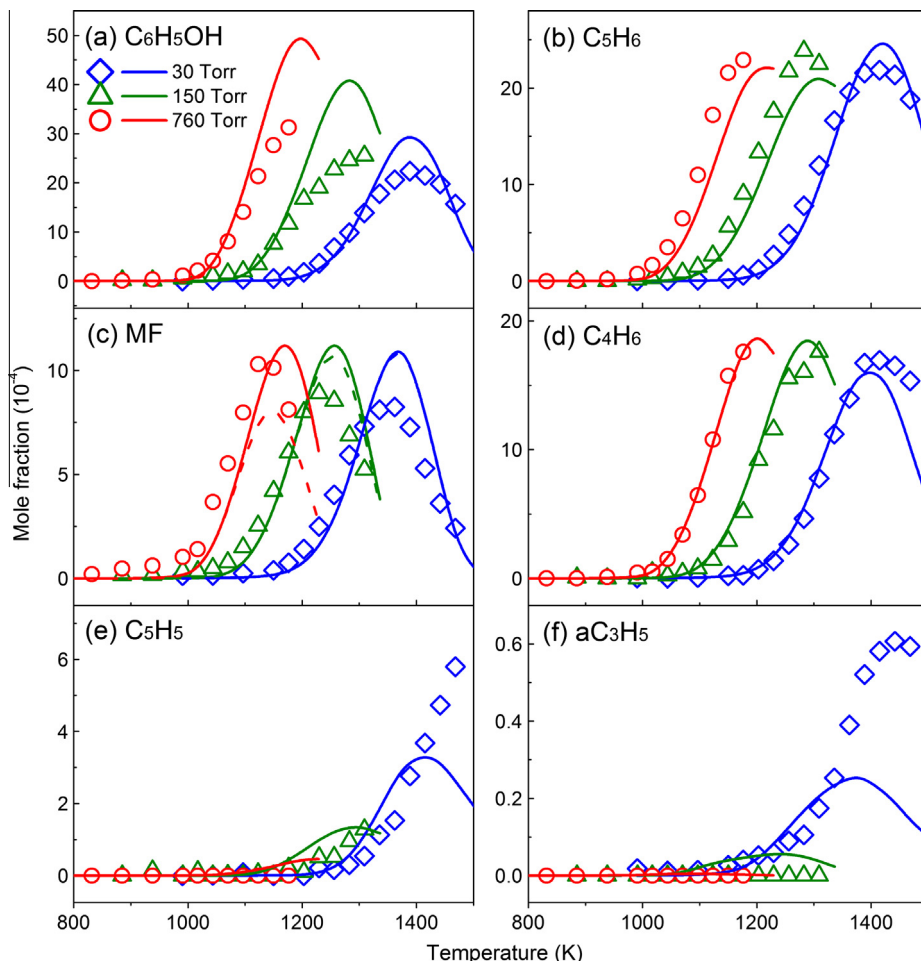


Fig. 6. Experimental (symbols) and simulated (lines) mole fraction profiles of (a) phenol (C₆H₅OH), (b) 1,3-cyclopentadiene (C₅H₆), (c) 2-methylfuran (MF), (d) 1,3-butadiene (C₄H₆), (e) cyclopentadienyl radical (C₅H₅) and (f) allyl radical (aC₃H₅) in DMF pyrolysis at various pressures. Dashed lines in Fig. 6c present the simulated results of MF before the optimization of rate constants of R12.

reaction sequence $R4C_6H_7O \rightarrow R6C_6H_7O \rightarrow R7C_6H_7O \rightarrow nC_5H_{14-1}$ can suffer a β -C–C scission reaction to form aC_3H_5 radical and C_2H_2 , which contributes 79% and 90% to the production of aC_3H_5 radical at 30 and 760 Torr, respectively. Experimental and simulated mole fraction profiles of C_5H_5 and aC_3H_5 radicals are shown in Fig. 6e and f, respectively.

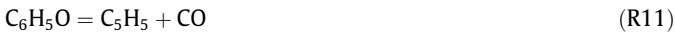
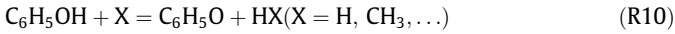


Figure 7 compares the simulated results of C_6H_5OH and C_5H_6 by the present model and the Sirjean and Somers models. It is observed that the two previous models over-predict the concentrations of C_6H_5OH and under-predict the concentrations of C_5H_6 at both 30 and 760 Torr. As mentioned above, Xu and Lin [58] performed a comprehensive theoretical investigation on the unimolecular decomposition of C_6H_5OH . A multiwell pathway was found to produce C_5H_6 and CO (R8) with the maximum energy transition state at 75.8 kcal/mol which is much lower than those of the O–H fission (89.1 kcal/mol) and dehydration (86.4 kcal/mol) pathways. However, R8 was not included in the Sirjean model [18] and its rate constant were divided by a factor of 2 in the Somers model [19], which is an important reason for the over-prediction of C_6H_5OH and under-prediction of C_5H_6 . Moreover, the comparison of the sensitivity analysis of C_5H_6 at 30 Torr by the present model and the Sirjean model [18] in Fig. 8 also reveals the importance of R8 to the formation of C_5H_6 .

Beside the H-atom abstraction reactions by small radicals, DMF can also be consumed by another two H-atom attack reactions (R5) and (R6), leading to the formation of MF + CH_3 and 1,3-butadiene (C_4H_6) + CH_3CO . The experimental and simulated mole fraction profiles of MF and C_4H_6 are shown in Fig. 6c and d, respectively. In the present model, the rate constants of R5 and R6 were taken

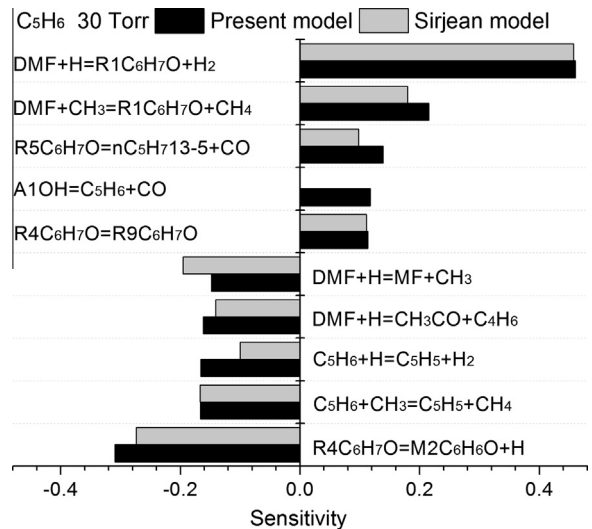


Fig. 8. Sensitivity analysis of C_5H_6 using the present model at 1389 K, 30 Torr and the Sirjean model at 1336 K, 30 Torr where the simulated conversions of DMF by the two models are very close to each other.

from the calculated results by Sirjean and Fournet [26], and the rate constant of R5 was divided by a factor of 1.5 considering the calculation uncertainties and the validation against the measured mole fraction profiles of MF in both the present work and previous pyrolysis work (e.g. Fig. 14b). The contributions of R5 and R6 to the consumption of DMF are quite similar to each other, and the contribution of each reaction only changes slightly from 30 Torr to 760 Torr. On the other hand, the two reactions are also the dominant formation pathways of MF and C_4H_6 , respectively. Furthermore, R6 is the other main formation pathway of CH_3CO radical beside R2, and consequently plays an important role in the formation of CH_3 radical and CO.

The decomposition reactions of MF are mainly taken from the MF model of Somers et al. [27]. The most important decomposition pathway of MF is the H-atom abstraction reactions by small radicals which produces 2-furyl methyl radical (furyl CH_2). During the validation of the present model, it was found that the simulated maximum mole fraction of MF decreased as the pressure increased (see the dash lines in Fig. 6c), which was contrary to the experimental trend. According to the ROP analysis, the problem was attributed to the unexpected high contributions of the H-atom abstraction of MF by C_5H_5 radical (R12) at elevated pressures. It is realized that in the MF [27] and DMF [19] models of Somers et al., the doubled rate constant of the H-atom abstraction of $C_6H_5CH_3$ by C_5H_5 radical [57] was used for R7 and R12. As mentioned above, the original rate constant of the $C_6H_5CH_3 + C_5H_5$ reaction in [57] were actually overestimated by -4 kcal/mol in the activation energy term. Therefore in the present model, R12 was referred to the calculated H-atom abstraction reaction of MF by aC_3H_5 radical [18], which is consistent with the Sirjean model. This enables the present model to capture the experimental trend of MF at different pressures. Besides, other main decomposition pathways of MF are similar to those in Somers et al. [27].



Figure 9 illustrates several important small C_2 – C_4 products in DMF pyrolysis, including diacetylene (C_4H_2), C_3H_3 radical, ethylene (C_2H_4) and C_2H_2 . As summarized in Fig. 3, these small products are all formed during the decomposition of aforementioned products. For C_4H_2 , its formation is dominated by the two-step H-atom-loss reaction sequence of C_4H_4 . C_3H_3 radical is mainly formed from the unimolecular decomposition reaction of C_5H_5 radical, and suffers

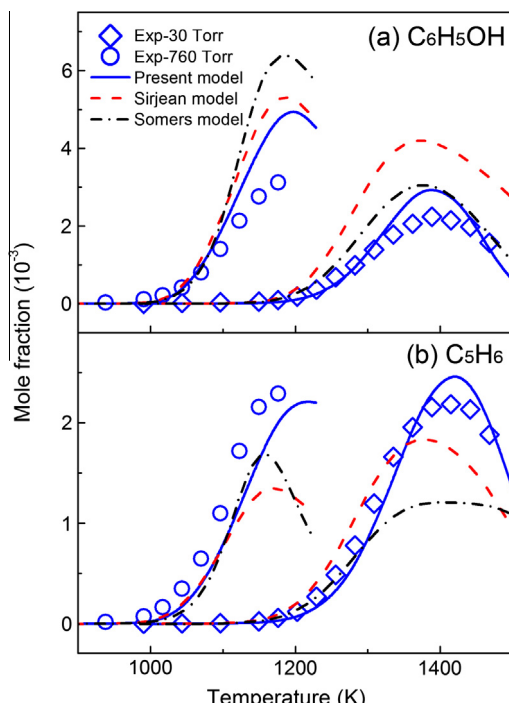


Fig. 7. Comparison of simulated mole fraction profiles of (a) C_6H_5OH and (b) C_5H_6 by the present model (solid lines), the Sirjean model (dash lines) and the Somers model (dash dot lines) with experimental results (symbols).

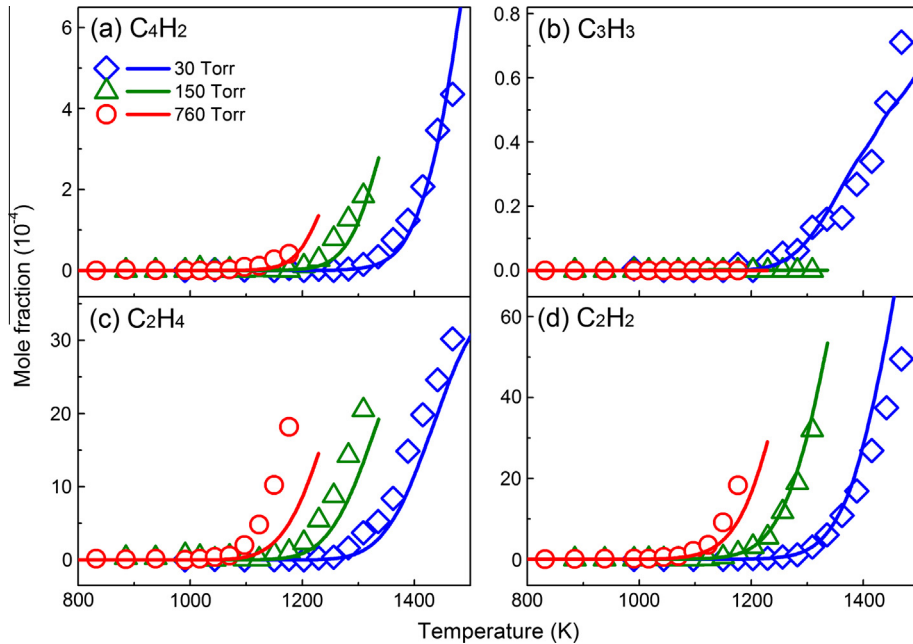


Fig. 9. Experimental (symbols) and simulated mole fraction profiles (lines) of (a) diacetylene (C_4H_2), (b) propargyl radical (C_3H_3), (c) ethylene (C_2H_4) and (d) acetylene (C_2H_2) in DMF pyrolysis at various pressures.

combination reactions with some decomposition products of DMF to generate larger products, especially aromatics. C_2H_4 and C_2H_2 are two major C_2 products in the present work. There are several main formation pathways of C_2H_4 , such as the H-atom attack on C_4H_6 and the β -C-H scission reaction of ethyl radical (C_2H_5) which is generated from CH_3 self-combination. C_2H_2 is mainly formed from the decomposition of larger species, such as $n\text{C}_5\text{H}_7$ 14-1 and C_5H_5 radicals.

5.1.2. Formation of aromatics

Beside the decomposition products, a series of aromatic hydrocarbons, including benzene (C_6H_6), $\text{C}_6\text{H}_5\text{CH}_2$ radical, $\text{C}_6\text{H}_5\text{CH}_3$,

phenylacetylene ($\text{C}_6\text{H}_5\text{C}_2\text{H}$), styrene ($\text{C}_6\text{H}_5\text{C}_2\text{H}_3$), C_9H_7 radical, indene (C_9H_8), naphthalene (C_{10}H_8) and so on, were also detected in the present work. Figures 10 and 11 show the experimental and simulated mole fraction profiles of these aromatic hydrocarbons. Figure 12 displays the reaction network in aromatics growth at 1389 K, 30 Torr and 1176 K, 760 Torr based on the ROP analysis.

Though DMF is a biomass-derived fuel with an oxygen atom, low carbonyl and specifically formaldehyde emissions were observed by Daniel et al. in a spark-ignition engine [15], revealing the potential advantage of DMF in reducing oxygenated pollutant emissions compared with alcohols. On the other hand, C_6H_6 was observed with very high concentrations in both the present work

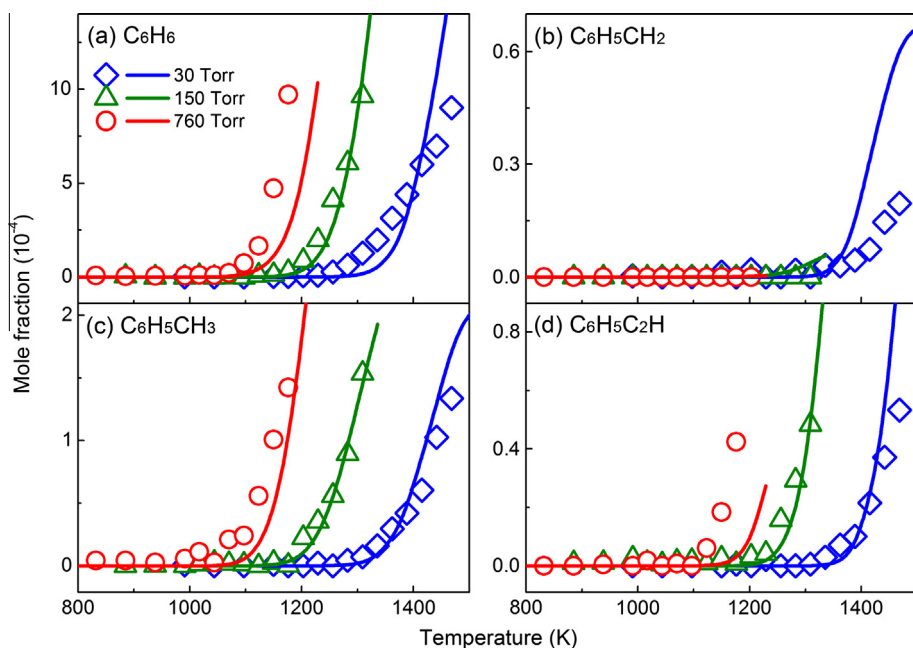


Fig. 10. Experimental (symbols) and simulated mole fraction profiles (lines) of (a) benzene (C_6H_6), (b) benzyl radical ($\text{C}_6\text{H}_5\text{CH}_2$), (c) toluene ($\text{C}_6\text{H}_5\text{CH}_3$) and (d) phenylacetylene ($\text{C}_6\text{H}_5\text{C}_2\text{H}$) in DMF pyrolysis at various pressures.

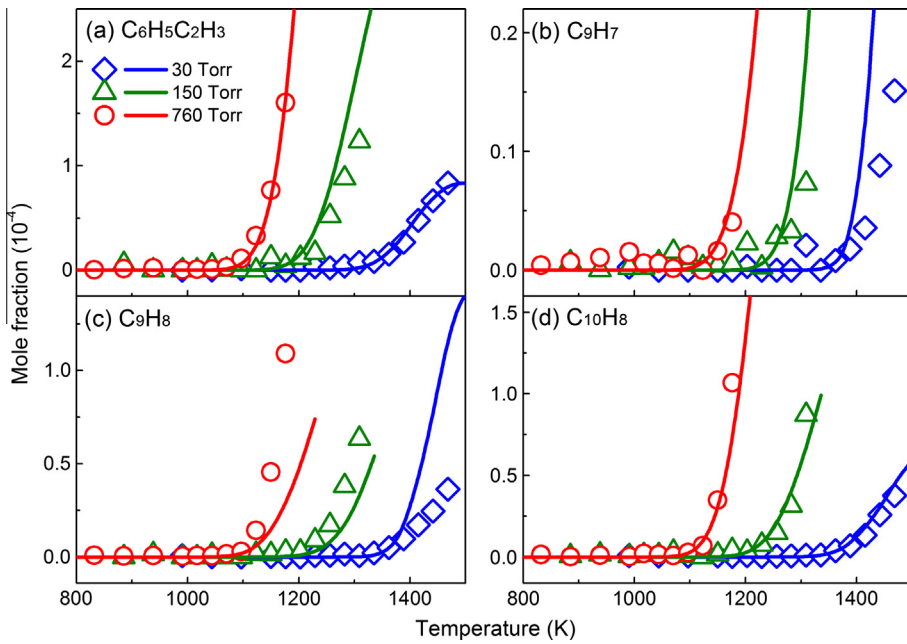


Fig. 11. Experimental (symbols) and simulated mole fraction profiles (lines) of (a) styrene ($C_6H_5C_2H_3$), (b) indenyl radical (C_9H_7), (c) indene (C_9H_8) and (d) naphthalene ($C_{10}H_8$) in DMF pyrolysis at various pressures.

and the previous rich premixed flame study of DMF by Togbe et al. [20]. Figure 13 compares the mole fractions of C_6H_6 at about 75% conversion of fuels in the present work and our previous pyrolysis studies of cyclohexane at 30 Torr [30] and methylcyclohexane at 30, 150 and 760 Torr [38]. In all studies, the inlet fuel mole fractions are 2% in argon. It can be observed that the formation of C_6H_6 was promoted in the pyrolysis of DMF compared with those in the pyrolysis of the two C_6-C_7 cycloalkanes. Togbe et al. [20] also

compared the yield of C_6H_6 in very rich premixed flames of DMF, MF, furan, *n*-butane, 1-butene, cyclohexane, dimethylether, ethanol, 1-butanol and methyl propanoate. Similarly, they observed that the maximum mole fraction of C_6H_6 in the DMF flame is much higher than those in other flames.

According to the ROP analysis, it is concluded that the formation of C_6H_6 is mainly controlled by the ipso substitution of C_6H_5OH by H-atom (R9) and a self-combination reaction of C_3H_3 radical (R13)

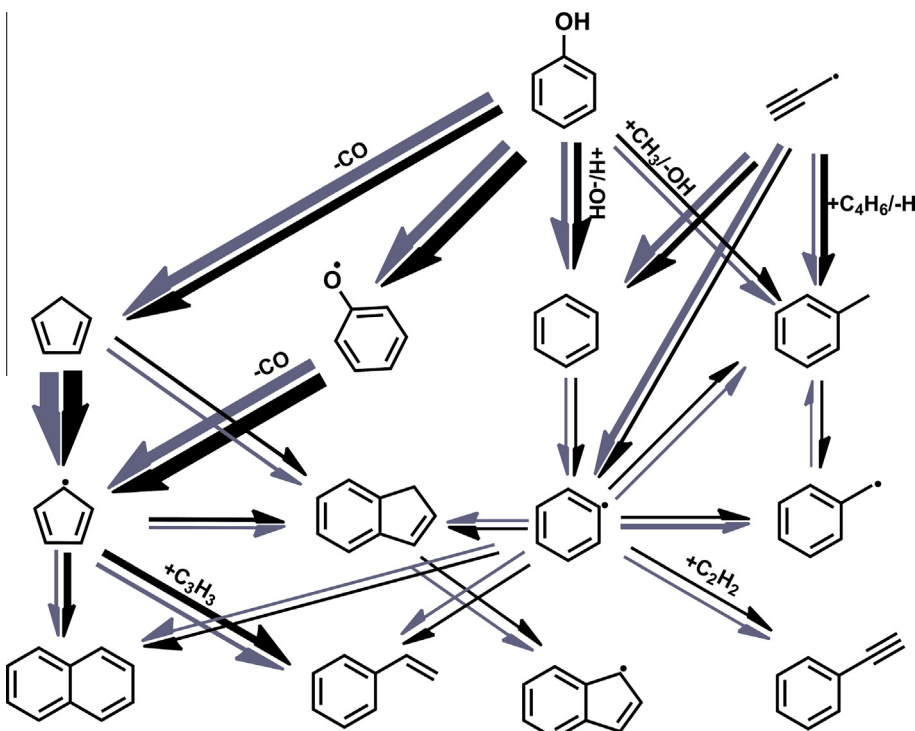


Fig. 12. Reaction network of aromatics growth at 1389 K, 30 Torr and 1176 K, 760 Torr. The arrow thicknesses are in a much smaller scale than those in Fig. 3.

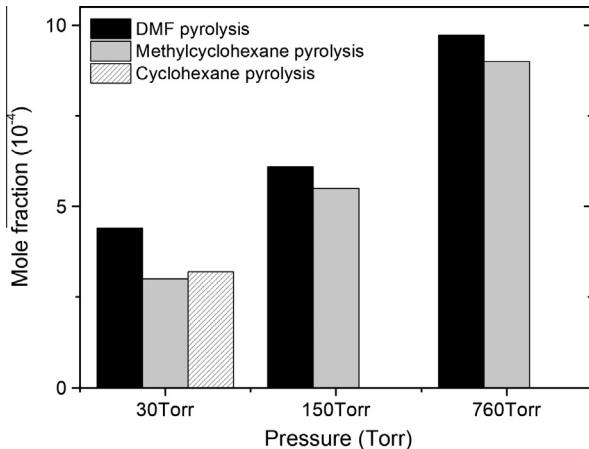
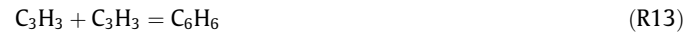


Fig. 13. Comparison of the mole fractions of C₆H₆ at about 75% conversion of DMF, cyclohexane (only 30 Torr) [30] and methylcyclohexane [38] with the same inlet mole fraction (2%) at 30, 150 and 760 Torr.

at both 30 and 760 Torr. In particular, R9 has high contributions at both pressures and dramatically enhances the formation of C₆H₆, which is consistent with the conclusion of Togbe et al. [20]. Therefore, the massive formation of C₆H₅OH in the pyrolysis and flames of DMF explains the high concentration levels of C₆H₆.

Additionally, the reaction of fulvene + H = C₆H₆ + H also has a minor contribution to the formation of C₆H₆ at both 30 and 760 Torr. The decomposition of C₆H₆ mainly proceeds through the H-atom abstraction reactions by small radicals to produce phenyl radical (C₆H₅) at both pressures, while the formation of C₆H₅ radical is dominated by another self-combination reaction of C₃H₃ radical (R14).



Two C₇ aromatics, C₆H₅CH₂ radical and C₆H₅CH₃ were detected in the present work. Their experimental and simulated mole fraction profiles are shown in Fig. 10b and c, respectively. C₆H₅CH₃ is mainly formed from the ipso substitution of C₆H₅OH by CH₃ radical (R15) and the reaction of C₃H₃ + C₄H₆ (R16) at both 30 and 760 Torr. In addition, C₆H₅CH₃ can also be formed from the association reactions of C₆H₅CH₂ + H and C₆H₅ + CH₃ (R17) and (R18) at 30 Torr. The H-atom abstraction of C₆H₅CH₃ by small radicals (R19) can produce C₆H₅CH₂ radical, which is the main formation pathway of C₆H₅CH₂ at 760 Torr. At 30 Torr, the formation of C₆H₅CH₂ radical is dominated by the reaction of C₆H₅ and CH₃ radicals (R20).

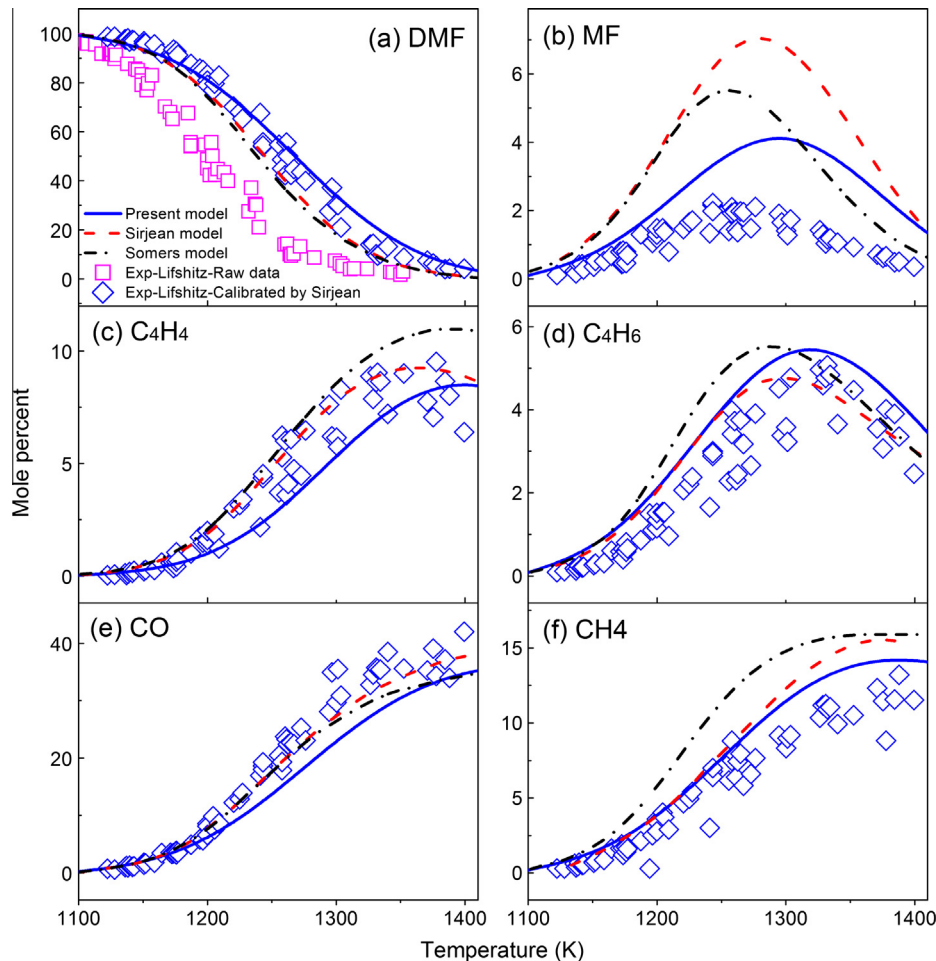
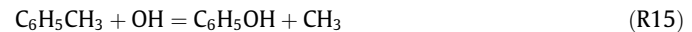
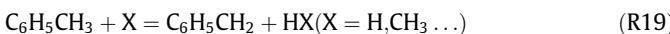
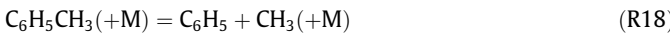
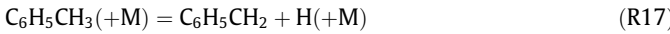


Fig. 14. Validation of the present model against shock tube pyrolysis results of 0.5% DMF in argon. Calibrated results of Lifshitz et al. [10] by Sirjean et al. [18] are used as experimental data (open diamonds), and are compared with simulated results by the present model (solid lines), the Sirjean models (dashed lines) and the Somers model (dash dot lines).



$\text{C}_6\text{H}_5\text{C}_2\text{H}$ and $\text{C}_6\text{H}_5\text{C}_2\text{H}_3$ are two typical C_8 aromatic products, and their experimental and simulated mole fraction profiles are displayed in Figs. 10d and 11a, respectively. Though the molecular structures of $\text{C}_6\text{H}_5\text{C}_2\text{H}$ and $\text{C}_6\text{H}_5\text{C}_2\text{H}_3$ are quite similar, their main formation pathways in the pyrolysis of DMF are different according to the ROP analysis. $\text{C}_6\text{H}_5\text{C}_2\text{H}$ is mainly formed from the reaction of $\text{C}_6\text{H}_5 + \text{C}_2\text{H}_2$ (R21) which is the second step of the hydrogen-abstraction-carbon-addition (HACA) pathway on C_6H_6 . $\text{C}_6\text{H}_5\text{C}_2\text{H}_3$ is the third abundant products among the eight aromatic products in Figs. 10 and 11, and its concentration is only lower than those of C_6H_6 and $\text{C}_6\text{H}_5\text{CH}_3$. The production of $\text{C}_6\text{H}_5\text{C}_2\text{H}_3$ is so promoted in the pyrolysis of DMF that its typical formation pathway from $\text{C}_6\text{H}_5 + \text{C}_2\text{H}_4$ (R22) was unable to explain its high concentration. Slavinskaya and Frank [59] proposed a combination reaction of C_5H_5 and C_3H_3 radicals (R23) in their aromatics formation mechanism, and referred it to the self-combination of C_3H_3 radical (R13) with their estimated rate constant. This reaction was also added to the present model. The rate constant was taken from the calculated results of R13 by Miller and Klippenstein [60], and was divided by a

factor of 5 considering the relatively high energy barrier from the five-member-ring adduct of $\text{C}_5\text{H}_5 + \text{C}_3\text{H}_3$ to the six-member-ring product $\text{C}_6\text{H}_5\text{C}_2\text{H}_3$. As a result of the high concentration levels of C_5H_5 and C_3H_3 radicals in the pyrolysis of DMF, the formation of $\text{C}_6\text{H}_5\text{C}_2\text{H}_3$ is controlled by R23 at both 30 and 760 Torr.

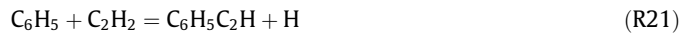


Figure 11 also exhibits three PAHs, including C_9H_7 radical, C_9H_8 and C_{10}H_8 . According to the ROP analysis, the formation of C_9H_8 is controlled by the reactions of $\text{C}_6\text{H}_5 + \text{C}_3\text{H}_3$ and $\text{C}_5\text{H}_5 + \text{C}_5\text{H}_6$ at 30 and 760 Torr, respectively. The main decomposition pathway of C_9H_8 is the H-atom abstraction by H-atom and CH_3 radical to produce C_9H_7 radical at both pressures. This pathway also controls the formation of C_9H_7 radical. Furthermore, the formation of C_{10}H_8 is mainly from the self-combination of C_5H_5 radical and the combination reaction of $\text{C}_6\text{H}_5 + \text{C}_4\text{H}_4$ at 30 Torr, and is dominated by the former reaction at 760 Torr.

Based on the discussion above, it is concluded that C_5H_5 radical, C_6H_5 radical and benzene are the most important precursors of large MAHs and PAHs in the pyrolysis of DMF. As a result, many aromatic products were detected in the present work and the previous pyrolysis work reported by Djokic et al. [16]. The present

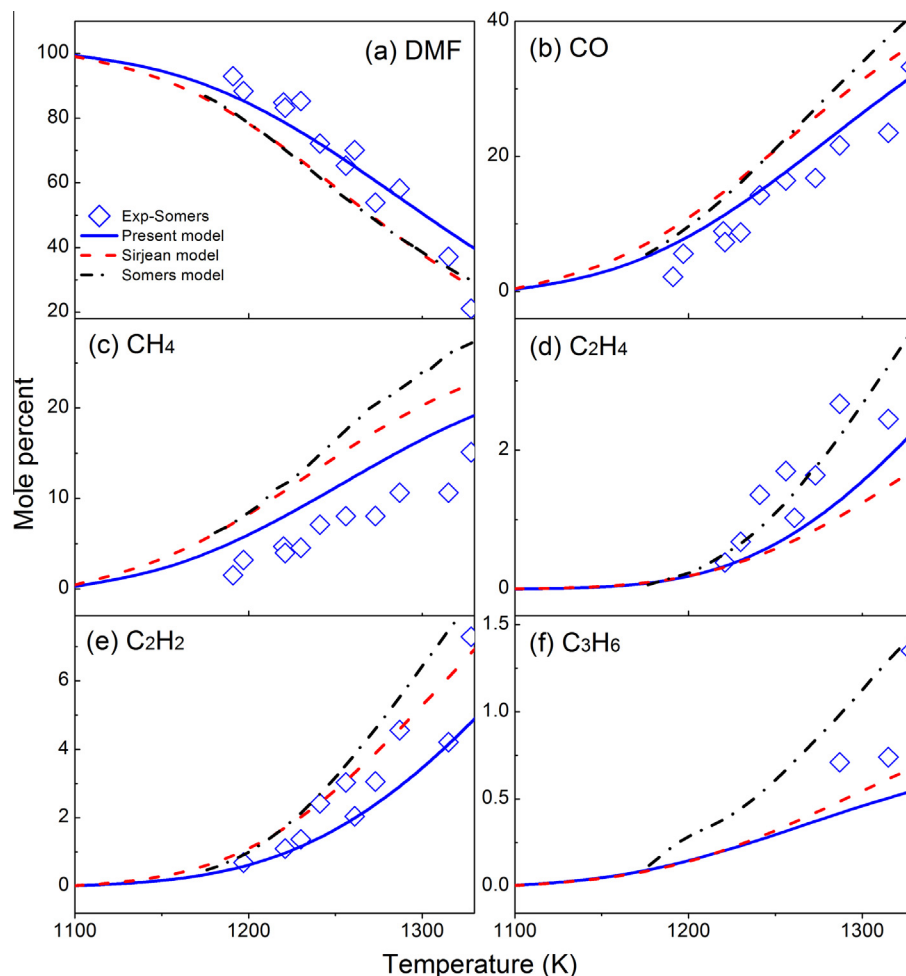


Fig. 15. Validation of the present model against shock tube pyrolysis results of 3% DMF in argon. Open diamonds are experimental data from Somers et al. [19], and lines are simulated results by the present model (solid lines), the Sirjean model (dashed lines) and the Somers model (dash dot lines).

work and the work of Togbe et al. [20] both concluded that the concentration levels of benzene in the combustion of DMF greatly exceed those in the combustion of many chain or cyclic hydrocarbons and oxygenated hydrocarbons under similar conditions. Furthermore, many large aromatics, such as $C_6H_5C_2H$, $C_6H_5C_2H_3$ and C_9H_8 , were also observed with higher concentrations in the present 30 Torr pyrolysis experiment of DMF than in the 30 Torr pyrolysis experiment of cyclohexane [30]. The experimental observations and modeling analysis imply that DMF has an intrinsic potential to generate high concentration levels of PAHs and consequently soot in combustion due to its special chemical structure.

However, it is noteworthy that the investigations on soot formation and emissions in the combustion of DMF are still insufficient. For example, though a lot of studies have been performed to investigate the sooting tendencies of various families of oxygenates such as alcohols, esters, ethers, aldehydes, and ketones [61–63], few efforts have been made to measure the sooting tendencies of furan family, which limits the evaluation of the sooting characteristics of furan family. Moreover, in a recent combustion and emission study of DMF in a compression-ignition engine [64], Chen et al. detected low soot emissions in DMF-diesel oil blends compared with *n*-butanol-diesel oil blends and gasoline-diesel oil blends due to the extended ignition delay. Therefore, comprehensive and systematic investigations on both laboratory and engine combustion of DMF, especially focusing on its sooting behavior and soot formation mechanism, are desired in the future to propel the application of DMF as an environment-friendly renewable fuel.

5.2. Validation of experimental data from literatures

The present model was also validated against the pyrolysis data from the shock tube pyrolysis experiments of DMF by Lifshitz et al. [10] and Somers et al. [19] and the flow reactor pyrolysis experiments of DMF by Djokic et al. [16]. The simulated results of DMF and several important products by the present model and the Sirjean and Somers models are shown in Figs. 14–16 for corresponding experiments. In the three previous experiments, the results of a specific species were expressed as its mole percent in all detected pyrolysis species beside the diluent gas. Therefore the simulated mole fraction profiles were converted to the mole percent profiles in order to be compared with the experimental results.

Lifshitz et al. [10] estimated the reflected shock temperatures by simulating the extent of the decomposition of 1,1,1-trifluoroethane which served as an internal chemical thermometer standard. However Sirjean et al. [18] found the underestimation of the reflected shock temperatures by Lifshitz et al. [10]. To solve the problem, they performed theoretical calculations on the decomposition of 1,1,1-trifluoroethane, and calibrated the reflected shock temperatures linearly towards higher temperature region. To verify this calibration, Somers et al. [19] performed a similar shock tube pyrolysis experiment of 3% DMF in argon with six products detected. They concluded that considering the experimental uncertainties, their new results are in reasonable agreement with the data of Lifshitz et al. [10] with calibrated temperatures. Therefore

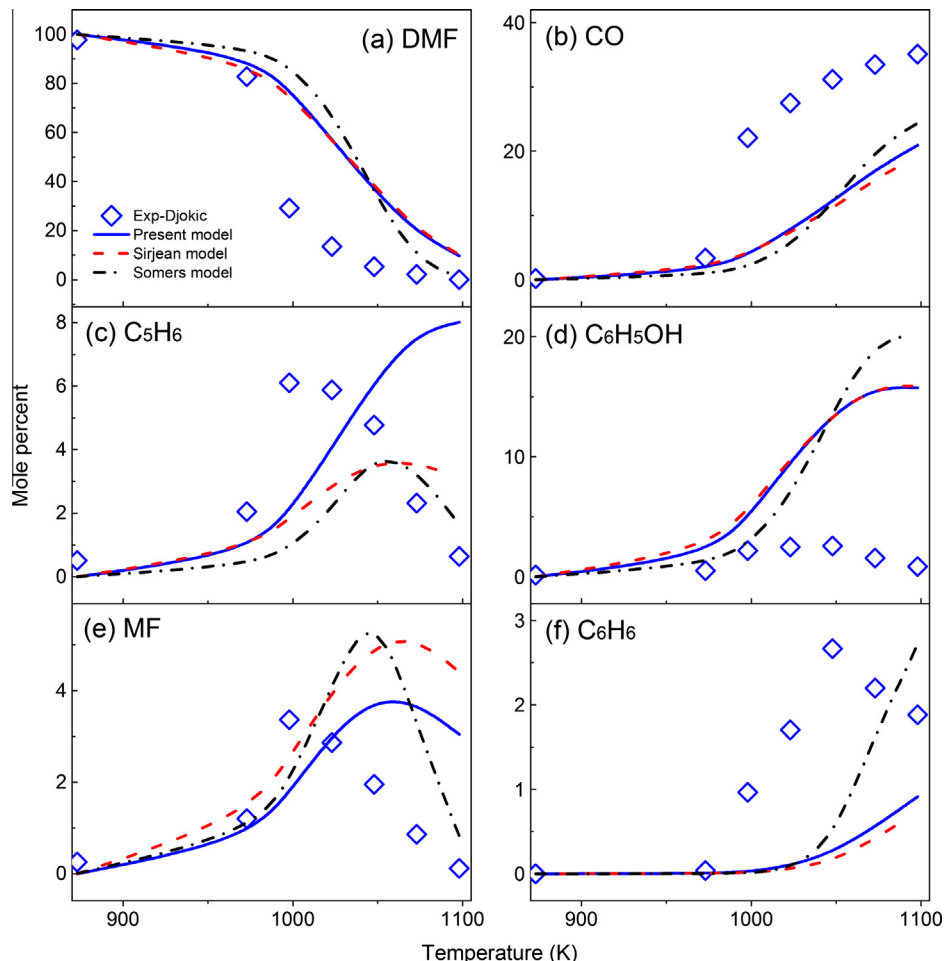


Fig. 16. Validation of the present model against flow reactor pyrolysis results of DMF at 1.7 bar from Djokic et al. [16]. Open diamonds denote the experimental data, and solid, dashed and dash dot lines denote the simulated results by the present model, the Sirjean model and the Somers model.

the calibrated temperatures are used in the validation here. As seen from Fig. 14a, the open squares represent the raw mole percent profile of DMF for 0.5% DMF in argon at the pressures of 2–3 atm and residence times of 1.8–2.3 ms in [10], and the open diamonds represent the calibrated data by Sirjean et al. [18]. It is observed that the present model can reproduce the experimental results of DMF and its decomposition products, especially the decomposition rate of DMF and the maximum mole percent of MF. In particular, both the closest simulation of MF to the experimental results among all models in Fig. 14b and the reproduction of measured MF profiles in the present work in Fig. 6c provide validation to the reduced rate constant of R5 in the present model. Besides, Fig. 15 shows the comparison of simulated results by all models with the experimental data from Somers et al. [19]. The performance of the present model in reproducing their experimental data is generally satisfactory.

Furthermore, the three models were also used to simulate the flow reactor pyrolysis data from Djokic et al. [16] at the pressure of 1.7 bar, temperatures of 873–1098 K and residence times of 300–400 ms, as shown in Fig. 16. The major problem between their experimental data and the simulated results is that all models cannot capture the abruptly accelerated decomposition of DMF and formation of products at around 1000 K in the experiment, while the three models generally behave well in reproducing the DMF profiles in the other pyrolysis experiments at 1–3 atm. Besides, all models over-predict the maximum mole percent of C₆H₅OH for almost an order of magnitude, while they are all able to predict the results of C₆H₅OH in the present experiment within a factor of 2 as shown in Fig. 7a. Somers et al. [19] also noticed these problems in the validation of their model against the data from Djokic et al. [16], and found that it is difficult to resolve the differences between the experimental results and their simulated results without significant performance loss against the shock tube experimental data. Since nickel based alloys (such as Incoloy 800HT used in [16]) have catalytic effects on hydrocarbon cracking and coke formation [65], they doubted whether the influence of surface catalyzed effects could be eliminated from the experimental results, and suggested the need of further analysis to solve the problem [19].

6. Conclusion

In the present work, the flow reactor pyrolysis of DMF at pressures of 30, 150 and 760 Torr was studied using SVUV-PIMS under the temperature range of 780–1470 K. The pyrolysis products were identified, and their mole fraction profiles were determined. In particular, phenol, 1,3-cyclopentadiene, 2-methylfuran, vinylacetylene and 1,3-butadiene were observed with high concentrations in the decomposition of DMF. The pressure-dependent rate constants of the major unimolecular decomposition reactions of DMF were calculated by using the Inverse Laplace Trans-form method in the MESMER code, and was adopted in the detailed pyrolysis model with 285 species and 1173 reactions developed in the present work. The model was validated against both the present work and the pyrolysis studies in literature. Generally, the present model can reproduce the results of most pyrolysis species within the experimental uncertainty at all investigated pressures. The ROP analysis and sensitivity analysis was performed to analyze the main reaction pathways in the pyrolysis of DMF. It is concluded that at both low and atmospheric pressures, the consumption of DMF is mainly controlled by the unimolecular decomposition to produce CH₃CHCCH and acetyl radicals, H-atom abstraction by H-atom and CH₃ radical to produce 5-methyl-2-furanylmethyl radical, ipso substitution by H-atom to produce MF and CH₃ radical, and H-atom attack to produce 1,3-butadiene and acetyl radical.

Great reaction flux from 5-methyl-2-furanylmethyl radical flows to phenol and 1,3-cyclopentadiene, which stimulates the formation of cyclopentadienyl radical, phenyl radical and benzene which are the precursors of large aromatics. As a result, the concentration levels of benzene and large aromatics in the pyrolysis of DMF are elevated compared with the pyrolysis of C₆–C₇ cycloalkanes under very close conditions, which implies the potentially high soot tendency of DMF. In future, more investigations on both laboratory and engine combustion of DMF, especially focusing on its soot behavior and soot formation mechanism, are desired for the potential application of DMF as an alternative engine fuel.

Acknowledgments

Authors are grateful for the funding support from National Natural Science Foundation of China (51036007, 51106146), National Basic Research Program of China (973 Program) (2013CB834602), Anhui Science & Technology Department (1408085J09), Fundamental Research Funds for the Central Universities (WK2320000020, WK2320000028) and Chinese Academy of Sciences. Authors are grateful to Long Zhao, Jiuzhong Yang, Wenhao Yuan, Yizun Wang and Zhandong Wang for their help.

Appendix A. Supplementary material

Supplementary data associated with this article can be found, in the online version, at <http://dx.doi.org/10.1016/j.combustflame.2014.03.022>.

References

- [1] Y. Roman-Leshkov, C.J. Barrett, Z.Y. Liu, J.A. Dumesic, *Nature* 447 (2007) 982–985.
- [2] H. Zhao, J.E. Holladay, H. Brown, Z.C. Zhang, *Science* 316 (2007) 1597–1600.
- [3] M. Mascal, E.B. Nikitin, *Angew. Chem. Int. Ed.* 47 (2008) 7924–7926.
- [4] L.S. Tran, B. Sirjean, P.A. Claude, R. Fournet, F. Battin-Leclerc, *Energy* 43 (2012) 4–18.
- [5] G.H. Tian, R. Daniel, H.Y. Li, H.M. Xu, S.J. Shuai, P. Richards, *Energy Fuels* 24 (2010) 3898–3905.
- [6] X.S. Wu, Z.H. Huang, X.G. Wang, C. Jin, C.L. Tang, L.X. Wei, C.K. Law, *Combust. Flame* 158 (2011) 539–546.
- [7] L.S. Tran, B. Sirjean, P.-A. Glaude, R. Fournet, F. Battin-Leclerc, *Energy* 43 (2012) 4–18.
- [8] J.M. Simmie, H.J. Curran, *J. Phys. Chem. A* 113 (2009) 5128–5137.
- [9] M.A. Grela, V.T. Amorebieta, A.J. Colussi, *J. Phys. Chem.* 89 (1985) 38–41.
- [10] A. Lifshitz, C. Tamburu, R. Shashua, *J. Phys. Chem. A* 102 (1998) 10655–10670.
- [11] X.S. Wu, Z.H. Huang, T. Yuan, K.W. Zhang, L.X. Wei, *Combust. Flame* 156 (2009) 1365–1376.
- [12] S.H. Zhong, R. Daniel, H. Xu, J. Zhang, D. Turner, M.L. Wyszynski, P. Richards, *Energy Fuels* 24 (2010) 2891–2899.
- [13] R. Daniel, G.H. Tian, H.M. Xu, M.L. Wyszynski, X.S. Wu, Z.H. Huang, *Fuel* 90 (2011) 449–458.
- [14] P. Friese, T. Bentz, M. Olzmann, J.M. Simmie, in: Proceedings of the European Combustion Meeting, Cardiff, UK, 2011.
- [15] R. Daniel, L.X. Wei, H.M. Xu, C.M. Wang, M.L. Wyszynski, S.J. Shuai, *Energy Fuels* 26 (2012) 6661–6668.
- [16] M. Djokic, H.-H. Carstensen, K.M. Van Geem, G.B. Marin, *Proc. Combust. Inst.* 34 (2013) 251–258.
- [17] P. Friese, J.M. Simmie, M. Olzmann, *Proc. Combust. Inst.* 34 (2013) 233–239.
- [18] B. Sirjean, R. Fournet, P.A. Glaude, F. Battin-Leclerc, W. Wang, M.A. Oehlschlaeger, *J. Phys. Chem. A* 117 (2013) 1371–1392.
- [19] K.P. Somers, J.M. Simmie, F. Gillespie, C. Conroy, G. Black, W.K. Metcalfe, F. Battin-Leclerc, P. Dirrenberger, O. Herbinet, P.-A. Glaude, P. Dagaut, C. Togbe, K. Yasunaga, R.X. Fernandes, C. Lee, R. Tripathi, H.J. Curran, *Combust. Flame* 160 (2013) 2291–2318.
- [20] C. Togbe, L.S. Tran, D. Liu, D. Felsmann, P. Osswald, P.A. Glaude, B. Sirjean, R. Fournet, F. Battin-Leclerc, K. Kohse-Hoinghaus, *Combust. Flame* 161 (2014) 780–797.
- [21] C.M. Wang, H.M. Xu, R. Daniel, A. Ghafourian, J.M. Herreros, S.J. Shuai, X. Ma, *Fuel* 103 (2013) 200–211.
- [22] J.M. Simmie, W.K. Metcalfe, *J. Phys. Chem. A* 115 (2011) 8877–8888.
- [23] D. Feller, J.M. Simmie, *J. Phys. Chem. A* 116 (2012) 11768–11775.
- [24] B. Sirjean, R. Fournet, *J. Phys. Chem. A* 116 (2012) 6675–6684.
- [25] B. Sirjean, R. Fournet, *Phys. Chem. Chem. Phys.* 15 (2013) 596–611.
- [26] B. Sirjean, R. Fournet, *Proc. Combust. Inst.* 34 (2013) 241–249.

- [27] K.P. Somers, J.M. Simmie, F. Gillespie, U. Burke, J. Connolly, W.K. Metcalfe, F. Battin-Leclerc, P. Dirrenberger, O. Herbinet, P.A. Glaude, H.J. Curran, Proc. Combust. Inst. 34 (2013) 225–232.
- [28] F. Qi, R. Yang, B. Yang, C.Q. Huang, L.X. Wei, J. Wang, L.S. Sheng, Y.W. Zhang, Rev. Sci. Instrum. 77 (2006) 084101.
- [29] Y.Y. Li, F. Qi, Acc. Chem. Res. 43 (2010) 68–78.
- [30] Z.D. Wang, Z.J. Cheng, W.H. Yuan, J.H. Cai, L.D. Zhang, F. Zhang, F. Qi, J. Wang, Combust. Flame 159 (2012) 2243–2253.
- [31] F. Qi, Proc. Combust. Inst. 34 (2013) 33–63.
- [32] C.R. Narayanan, S. Srinivasan, A.K. Datye, R. Gorte, A. Biaglow, J. Catal. 138 (1992) 659–674.
- [33] M. Cathonnet, J.C. Boettner, H. James, Proc. Combust. Inst. 18 (1981) 903–913.
- [34] P. Glarborg, P.G. Kristensen, S.H. Jensen, K. Dam-Johansen, Combust. Flame 98 (1994) 241–258.
- [35] P.G. Kristensen, P. Glarborg, K. Dam-Johansen, Combust. Flame 107 (1996) 211–222.
- [36] Y.J. Zhang, J.H. Cai, L. Zhao, J.Z. Yang, H.F. Jin, Z.J. Cheng, Y.Y. Li, L.D. Zhang, F. Qi, Combust. Flame 159 (2012) 905–917.
- [37] J.H. Cai, L.D. Zhang, F. Zhang, Z.D. Wang, Z.J. Cheng, W.H. Yuan, F. Qi, Energy Fuels 26 (2012) 5550–5568.
- [38] Z.D. Wang, L.L. Ye, W.H. Yuan, L.D. Zhang, Y.Z. Wang, Z.J. Cheng, F. Zhang, F. Qi, Combust. Flame 161 (2014) 84–100.
- [39] L.B. Harding, S.J. Klippenstein, Y. Georgievskii, J. Phys. Chem. A 111 (2007) 3789–3801.
- [40] W. Tsang, R.F. Hampson, J. Phys. Chem. Ref. Data 15 (1986) 1087–1279.
- [41] W. Tsang, J. Phys. Chem. Ref. Data 19 (1990) 1–68.
- [42] W. Tsang, J. Phys. Chem. Ref. Data 17 (1988) 887–952.
- [43] S.J. Klippenstein, L.B. Harding, Y. Georgievskii, Proc. Combust. Inst. 31 (2007) 221–229.
- [44] S.H. Robertson, M.J. Pilling, D.L. Baulch, N.J.B. Green, J. Phys. Chem. 99 (1995) 13452–13460.
- [45] D.R. Glowacki, C.-H. Liang, C. Morley, M.J. Pilling, S.H. Robertson, J. Phys. Chem. A 116 (2012) 9545–9560.
- [46] S.H. Robertson, D.R. Glowacki, C.H. Liang, C. Morley, R. Shannon, M. Blitz, M.J. Pilling, MESMER (Master Equation Solver for Multi-Energy Well Reactions), <<http://sourceforge.net/projects/mesmer>>.
- [47] M.J. Frisch, G.W. Trucks, H.B. Schlegel, G.E. Scuseria, M.A. Robb, J.R. Cheeseman, G. Scalmani, V. Barone, B. Mennucci, G.A. Petersson, H. Nakatsuji, M. Caricato, X. Li, H.P. Hratchian, A.F. Izmaylov, J. Bloino, G. Zheng, J.L. Sonnenberg, M. Hada, M. Ehara, K. Toyota, R. Fukuda, J. Hasegawa, M. Ishida, T. Nakajima, Y. Honda, O. Kitao, H. Nakai, T. Vreven, J.A. Montgomery, Jr., J.E. Peralta, F. Ogliaro, M. Bearpark, J.J. Heyd, E. Brothers, K.N. Kudin, V.N. Staroverov, T. Keith, R. Kobayashi, J. Normand, K. RagHAVACHARI, A. Rendell, J.C. Burant, S.S. Iyengar, J. Tomasi, M. Cossi, N. Rega, J.M. Millam, M. Klene, J.E. Knox, J.B. Cross, V. Bakken, C. Adamo, J. Jaramillo, R. Gomperts, R.E. Stratmann, O. Yazev, A.J. Austin, R. Cammi, C. Pomelli, J.W. Ochterski, R.L. Martin, K. Morokuma, V.G. Zakrzewski, G.A. Voth, P. Salvador, J.J. Dannenberg, S. Dapprich, A.D. Daniels, O. Farkas, J.B. Foresman, J.V. Ortiz, J. Cioslowski, D.J. Fox, Gaussian09, Revision B.01, Gaussian Inc., Wallingford CT, 2010.
- [48] Y.-R. Luo, Comprehensive Handbook of Chemical Bond Energies, CRC Press, Boca Raton, FL, 2007.
- [49] G. da Silva, J.A. Cole, J.W. Bozzelli, J. Phys. Chem. A 113 (2009) 6111–6120.
- [50] B.E. Poling, J.M. Prausnitz, J.P. O'Connell, The Properties of Gases and Liquids, McGraw-Hill, New York, 2001.
- [51] J.H. Cai, W.H. Yuan, L.L. Ye, Z.J. Cheng, Y.Z. Wang, L.D. Zhang, F. Zhang, Y.Y. Li, F. Qi, Combust. Flame 160 (2013) 1939–1957.
- [52] Y.Y. Li, J.H. Cai, L.D. Zhang, T. Yuan, K.W. Zhang, F. Qi, Proc. Combust. Inst. 33 (2011) 593–600.
- [53] Y.Y. Li, J.H. Cai, L.D. Zhang, J.Z. Yang, Z.D. Wang, F. Qi, Proc. Combust. Inst. 33 (2011) 617–624.
- [54] Y.Y. Li, L.D. Zhang, Z.D. Wang, L.L. Ye, J.H. Cai, Z.J. Cheng, F. Qi, Proc. Combust. Inst. 34 (2013) 1739–1748.
- [55] Z.Y. Tian, T. Yuan, R. Fournet, P.A. Glaude, B. Sirjean, F. Battin-Leclerc, K.W. Zhang, F. Qi, Combust. Flame 158 (2011) 756–773.
- [56] CHEMKIN-PRO 15092, Reaction Design, San Diego, 2009.
- [57] R. Bounaceur, I. Da Costa, R. Fournet, F. Billaud, F. Battin-Leclerc, Int. J. Chem. Kinet. 37 (2005) 25–49.
- [58] Z.F. Xu, M.C. Lin, J. Phys. Chem. A 110 (2006) 1672–1677.
- [59] N.A. Slavinskaya, P. Frank, Combust. Flame 156 (2009) 1705–1722.
- [60] J.A. Miller, S.J. Klippenstein, J. Phys. Chem. A 107 (2003) 7783–7799.
- [61] P. Pepiot-Desjardins, H. Pitsch, R. Malhotra, S.R. Kirby, A.L. Boehman, Combust. Flame 154 (2008) 191–205.
- [62] C.S. McEnally, L.D. Pfefferle, Environ. Sci. Technol. 45 (2011) 2498–2503.
- [63] E.J. Barrientos, M. Lapuerta, A.L. Boehman, Combust. Flame 160 (2013) 1484–1498.
- [64] G.S. Chen, Y.G. Shen, Q.C. Zhang, M.F. Yao, Z.Q. Zheng, H.F. Liu, Energy 54 (2013) 333–342.
- [65] L.L. Crynes, B.L. Crynes, Ind. Eng. Chem. Res. 26 (1987) 2139–2144.
- [66] Y. Sakai, A. Miyoshi, M. Koshi, W.J. Pitz, Proc. Combust. Inst. 32 (2009) 411–418.
- [67] Y.Z. He, W.G. Mallard, W. Tsang, J. Phys. Chem. 92 (1988) 2196–2201.
- [68] I.D. Costa, R. Fournet, F. Billaud, F. Battin-Leclerc, Int. J. Chem. Kinet. 35 (2003) 503–524.
- [69] H.H. Carstensen, A.M. Dean, Int. J. Chem. Kinet. 44 (2012) 75–89.
- [70] T. Seta, M. Nakajima, A. Miyoshi, J. Phys. Chem. A 110 (2006) 5081–5090.
- [71] A. Laskin, H. Wang, C.K. Law, Int. J. Chem. Kinet. 32 (2000) 589–614.
- [72] M.A. Oehlschlaeger, D.F. Davidson, R.K. Hanson, J. Phys. Chem. A 110 (2006) 9867–9873.
- [73] W.K. Metcalfe, S. Dooley, F.L. Dryer, Energy Fuels 25 (2011) 4915–4936.
- [74] A. Fahr, S.E. Stein, Proc. Combust. Inst. 22 (1989) 1023–1029.